MSc Graduation Project

Control of Magnetic Bearings in Wind Turbines

Tianyi Zhang

Supervisor: **Dr. ir. H. Polinder**

Daily supervisor: **Ghanshyam Shrestha**

April 2010

Committee Members

Prof. dr. eng. J. A. Ferreira

Dr. ir. H. Polinder

Dr. ir. Madeleine Gibescu

Acknowledgment

The works presented in this thesis can not be done without many help of individuals. I would like to thank everyone who provided help to me.

First of all, I would like to express my deepest gratitude to my supervisor, Henk Polinder, associate Professor of TU Delft, for his continuous guidance and support. I benefited a lot from his expertise, criticism and encouragement.

Additionally, I would like to thank my daily supervisor Ghanshyam Shrestha, PhD student of TU Delft. I really appreciate his constant support, help and patient during the entire thesis work. What I learned from him is not only academic knowledge, but also academic way to thinking.

Lots of thanks go to R. Schoevaars, who provides a lot of technical supporting during this project.

I would like to thank Alesssndro Abate, assistant Porfessor of Delft Center for System and Control, for his valuable suggestions in the start of this thesis.

Special gratitude goes to my good friend Zhe Cong, PhD student of Delft Center for System and Control. He gave me lots of help and suggestion in the end of the project.

Without friends, I can not survive in a country which is thousands of kilometers away from home. Therefore, I want to express my thanks to all my friends in Delft, Ruimin Yang, Chi Liu, Daoxin Li, Xiaolei Cui, Lu Nie, Guange Ge, Xiaodong Guo, Deheng Liu, Xiao Zhang, Jing Jin, Xin Xu, HuiFei Jin, Yang Xu and Leake Weldemariam for your support and friendship. I want to thank my brother Su Zhang. I really appreciate you always stand beside me. I can not go through such hard time without your support.

Moreover, I would like to thank my friends in China, Bo Xu, Jiangtian Chen, Jie Yang, Jie Chen, Fancao Kong, and Tianxin Zhu, for your support and encouragement.

Most importantly, I would like to express my strongest gratitude to my parents, who always support me and love me throughout my time in Delft.

Tianyi Zhang

Delft University of Technology

Abstract

Direct drive generators applied to large wind turbines present some problems, such as very heavy and expensive price. The use of magnetic bearings has a possibility to reduce the weight of the direct drive generator. The control system for such magnetic bearings is considered.

In the beginning, the thesis discusses the problems of direct drive generators in large wind turbines, introduces a hybrid concept of active magnetic bearings, gives a demonstrator of magnetic bearings used in this project, and presents a basic control system of active magnetic bearings.

For the purpose of support such magnetic bearings in wind turbines, this thesis gives a complete control system. This control system includes electrical circuits and decentralized control method. The implementation of the electrical circuits is distributed into two PCBs. The decentralized control method is designed with six PID controllers.

Finally, in order to improve the stability of the system, the H-infinity control method is suggested to magnetic bearing system in wind turbine applications.

Content

Chapter 1 Introduction

1.1 Wind Energy

Wind energy is a kind of renewable energy, and we have used it for hundreds of years. The kinetic energy of wind can be converted into other useful forms of energy, such as electricity, using wind turbines. Nowadays, two kinds of wind turbines are used to transfer wind energy to electricity. Onshore wind energy is commonly used worldwide, but it takes a large land use. However, the offshore wind energy performs better than onshore energy. The higher wind speed on the sea makes the wind turbines produce more electricity. So there is an increased interest in offshore wind turbines.

Recently, wind energy has been growing faster than before in the world. Both onshore and offshore wind farms are being planed and built in the past few years. Until now the biggest offshore wind farm is Horns Rev 2 in Denmark with 209 megawatt (MW) of installated power [1].

1.2 Comparison of Wind Turbine Generators

As the technology of modern wind turbines matures, there are two different concepts of generator have been used. The first one is a wind turbine generator with gearbox which has been used more. The second one is called direct-drive generator which recently got a lot of attention in wind turbine applications. There are some overview papers about these two types of generators. H. Polinder gave a nice comparison of five different generator systems in wind turbines [24]. Similarly the other paper had a review of generator system for direct-drive generator [25]. These two papers gave some introductions on the direct-drive generator and geared generator. Compared them, the advantages and disadvantages are shown in table 1-1.

Table 1-1 comparison direct-drive and geared generators.

Type of generators	Direct-drive generator	Geared generator
Advantages	Highest energy yield Less components and lower speed Less maintenance	Lower cost Simpler
Disadvantages	Large, heavy and expensive	Gearbox fails a lot and take a lot of time to replace

From the figure below, we can see the weight of direct drive machine increases rapidly as the size of the wind turbine increases.

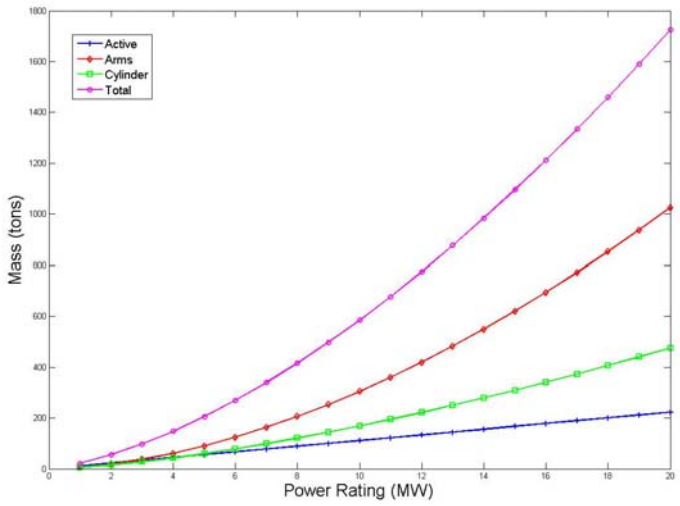

Figure 1.1 Estimated weight of direct drive machine of 1-20MW [2]

1.3 Magnetic Bearings and Control System

1.3.1 Active Magnetic Bearings

Considering the drawbacks of direct drive generators, we introduce magnetic bearings into this concept. A magnetic bearing is a bearing which supports a load using magnetic levitation. Magnetic bearings support moving machinery without physical contact, they can levitate a rotation shaft or permit relative motion without friction or wear.

There are different kinds of magnetic bearings. Here, in our design, we choose active magnetic bearings. An active magnetic bearing consists of an electromagnet, an amplifier which supplies current to the electromagnets, a controller, and a sensor with associated electronics to provide the feedback required to control the position of the rotor. This basic structure of active magnetic bearing is shown in figure 1.2.

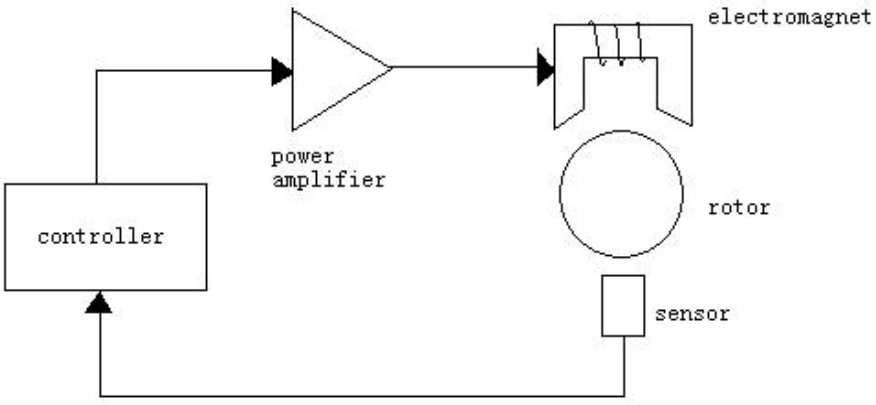

Figure 1.2 Basic elements of an active magnetic bearing

There are a lot of advantages of active magnetic bearing:

- Magnetic bearings can supply the rotor without mechanical contact, so the mechanical losses can be neglected.
- Magnetic bearings can add flexibility to wind turbine, this may reduce the weight of wind turbines.

On the other hand, the design of active magnetic bearing is much more complex.

1.3.2 Hybrid Concept

From the research of Ghanshyam Shrestha, there are three different wind turbine concepts using magnetic bearings that were investigated in [3].

The first one is single magnetic bearing, which use magnetic bearings to instead of mechanical bearings, then generator and wind turbine hub are fully levitated. The second concept is to have a rotor made of thin cylindrical ring which supported by amount of controlled magnetic actuators. More details of analyses in these two concepts can be found in [3] and [4]. Considering the single magnetic bearing concept has the problem of structure weight and the flexible rotor concept has a complicated control design. Therefore a hybrid concept as the last one has been introduced. The configuration of this concept is shown in figure 1.3.

In this construction the mechanical bearings takes the wind loads and transfer it to the tower. The magnetic bearings keep the air-gap of the machine and control the rotor in 5 degree of freedoms. Torque carrier carries the torque from wind turbine to the generator and only single directional force.

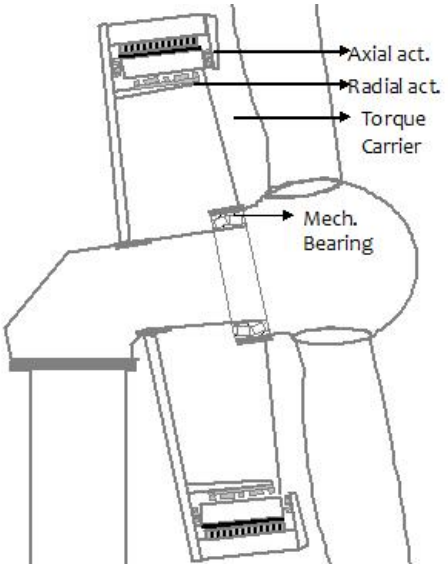

Figure 1.3 A hybrid concept configuration

Compared to the conventional machine, this concept eliminates the arms. From figure 1.1, the arms of machine are the major weight component. So eliminating them can reduce the weight of the direct drive machine substantially. Apart from this, this concept will also give some more flexibility. This concept of magnetic bearing design is used in this thesis, and the demonstrator as shown in figure 1.4, is being built to demonstrate the concept.

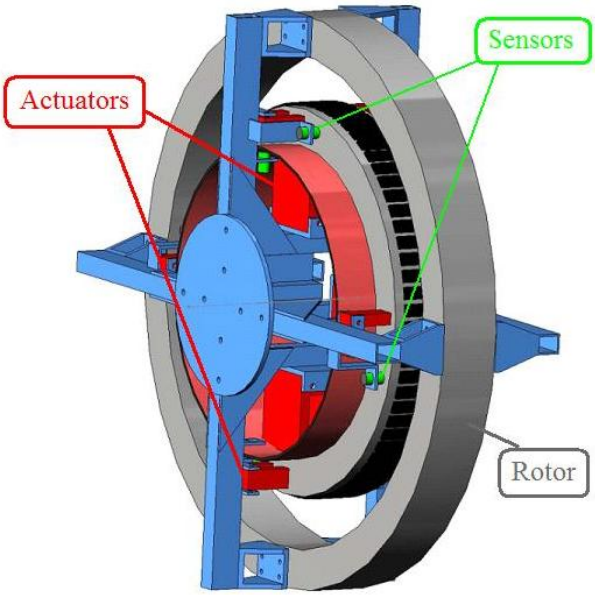

Figure 1.4 The basic structure of magnetic bearing

In this system, we have six pairs of actuators, six sensors, twelve amplifiers and six controllers. But this figure does not mention the amplifiers and controllers. Actuators and sensors are used to position the rotor. The magnetic force in actuators will change if the distances between rotor and actuator changes. Power amplifier transforms the control signal to a control current which generates a magnetic force in such a way to keep the rotor rotating in stable. Moreover, the controller controls the current i_x with a feedback of the position x to keep the rotor levitated.

1.3.3 Control System of Magnetic Bearings

For supporting such magnetic bearings mentioned above, we need a control system to control the rotor rotation. From figure 1.2 as shown before, we can see the work principle of such a control system. A sensor measures the displacement of the rotor from its reference position, a microprocessor as a controller derives a control signal from the measurement, a power amplifier transforms this control signal into a control current, and the control current generates a magnetic field in the actuating magnets, resulting in magnetic forces in such a way that the rotor remains in its hovering position.

In this control system, the important thing is to choose a suitable control method and a controller. This will be discussed in details in chapter 4.

1.4 Thesis Objective

The main objective of this thesis is to design a suitable control system for magnetic bearings in wind turbines. This main target includes two parts:

1) Design a control system for the demonstrator with magnetic bearings.
2) Get the first levitation of the magnetic bearing setup.

At the end of this thesis, a suggestion of another control method will be introduced which may be more suitable for such a system in wind turbine applications.

1.5 Thesis Layout

To get the main target of this thesis, the following steps need to be covered as well:

1) A literature review on applications of active magnetic bearings and suitable control algorithms for active magnetic bearings are shown in chapter 2.
2) A mathematical model of rotor and actuator with/without gyroscopic effect, is described in chapter 3.
3) This system is designed in decentralized control with a separate PID controller, and chapter 4 focuses on this part.
4) Chapter 5 talks about the performance of the setup.
5) In the end of this thesis, suggestion for a better control method for such a system is given.

Chapter 2 Literature Review

2.1 Applications of Magnetic Bearings

Active magnetic bearings can be used in several specialized applications such as:

· In transportation field. The magnetically levitated vehicle (MAGLEV), which uses electromagnetic principle, is a system of transportation. MAGLEV is suspended without any contact by several magnets from the iron tracks. Magnetic wheel, an important element of MAGLEV, is shown in figure 2.1[8] [5]. The highest recorded speed of a MAGLEV train is 581 kilometers per hour (361 mph), achieved in Japan in 2003 [9].

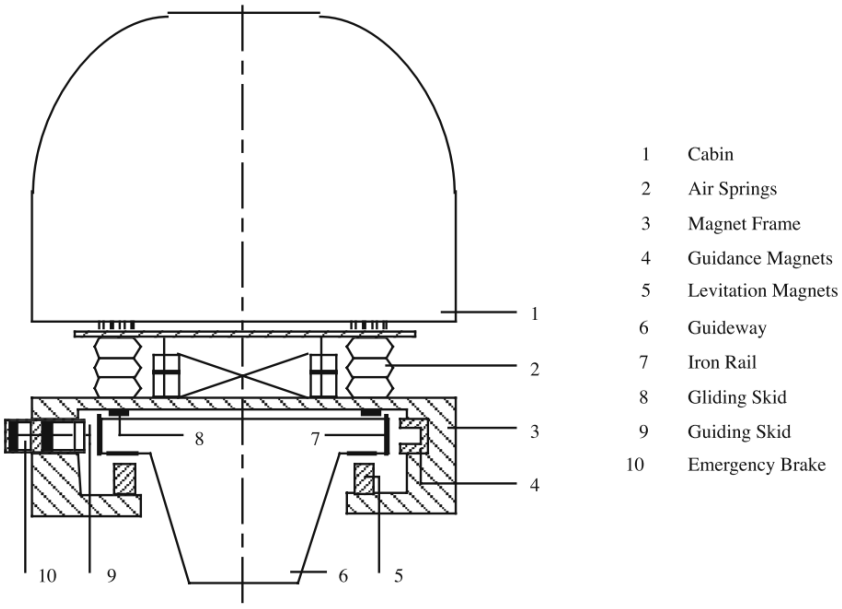

Figure 2.1 Scheme of a MAGLEV

- In industry field AMB are used in semiconductor industry, precision engineering and turbo-machinery. An example of turbo-generator for a nuclear power plant is shown in fig. 2.2.
- In medical applications AMB are useful as a left-ventricular assist device (LVAD) commonly known as an artificial heart is being researched [12].
- In aerospace applications AMB can be used for momentum wheels and for energy storage flywheels.

The examples, shown in figure 2.1 through 2.4 demonstrate recent products and developments of active magnetic bearings.

Figure 2.2 Schematic cross-section of a turbo-generator for a nuclear power plant, the first pebble-bed high temperature gas-cooled test reactor with the gas turbine in the direct cycle (HTR-10GT,under construction, Chinese government key project):6 MW, 15000 rpm, vertical rotor axis, 4 radial bearings,2 axial bearings, length of turbine 3.5 m, mass of turbine 1000 kg. (photo courtesy Institute of Nuclear and Novel Energy Technology INET, Tsinghua University, Beijing, [11]).

Figure 2.3 Turbo-blower: cooling gas compressor (CO_2) for a power laser, cutting a metal sheets up to 25mm. The laser needs uncontaminated gas. The speed is 54000 rpm, the rotor mass 3.6 kg, the motor power 12 KW, the radial bearing 48 mm in diameter, the bearing force 230 N (photo courtesy TRUMPF/MECOS) [10].

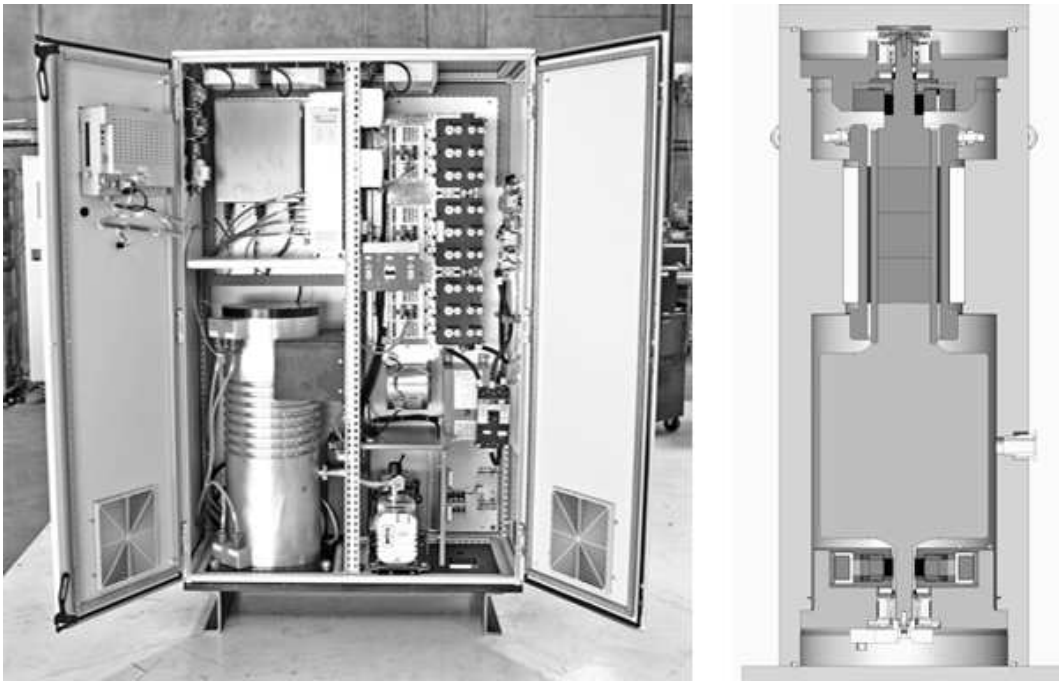

Figure 2.4 Flywheel: The 140 kW energy storage flywheel has been developed to provide 15 seconds of ride-through power and UPS service in conjunction with a diesel generator set. The flywheel operates in a vacuum. In the cabinet the flywheel is on the lower left, the magnetic bearing controller is at upper middle, motor/generator and system controller on upper left, and motor/generator power electronics on the right. The right figure shows the cross-section of the flywheel: total energy storage 1.25 kWh at 36000 rpm for delivery of 140 kW for 15 s (0.58 kWh), flywheel rotor mass 109 kg. The flywheel has a steel hub, a 2-pole brushless DC motor/generator, and permanent magnet biased magnetic bearings (courtesy CALNETIX) [17].

2.2 Control Design Methods for Magnetic Bearings

In this section, some important control design methods for active magnetic bearing systems are introduced. First, gives an initial introduction of these two methods at present. Furthermore, a short overview over some well-know but rarely applied control design methods is shown in the end of this section.

2.2.1 PID Control

PID is an acronym for "proportional, integral, derivative". A PID controller is a controller with these three elements. The PID controller was first introduced to the market in 1939 and remained the most widely used controller in industrially until today [13]. In 1989, an investigation of Japan performed that PID controller and advanced PID controller are used in more than 90% of process industries.

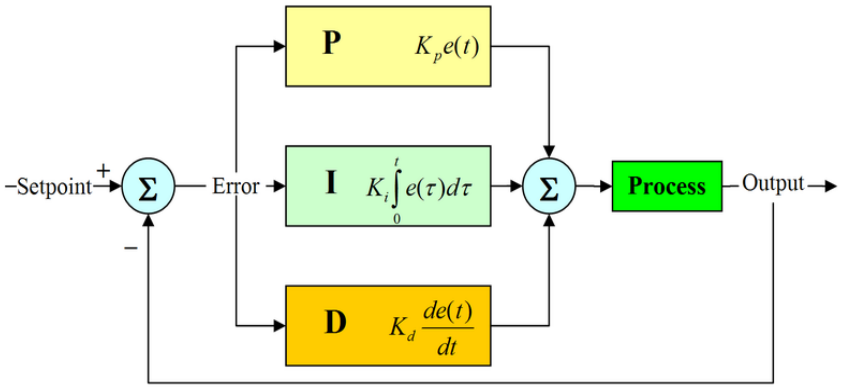

Figure 2.5 A block diagram of a PID controller

A PID controller is used to minimize the error between a measured process and a desired set point. As shown in figure2.5, a PID controller includes three separate parameters: the proportional, the integral, and the derivative.

A proportional term can be used to reduce the rise time, but never eliminate the steady-state error. The proportional response can be adjusted by multiplying the error by a constant K_p and it is given by:

$$P_{out} = K_p e(t) \qquad (2.1)$$

Where, P_{out} is proportional term of output. K_p is proportional gain and this K_p will make the system working quickly. e is the error of feedback. When the change in error is given, a high proportional gain results a large change in the output. If the proportional gain is too high, the system is becoming unstable.

An integral tem has the effect of eliminating the steady-state error, and also works on the speed of the system, but make the transient response worse. The magnitude of the contribution of the integral term to the overall control action is determined by the integral gain K_i, and it is given by:

$$I_{out} = K_i \int_0^t e(\tau)d\tau \qquad (2.2)$$

Where, I_{out} is integral term of output.

A derivative term increases the stability of the system, reducing overshoot and improving the transient response. The rate of change of the process error is calculated by determining the slope of the error over time and multiplying this rate of change by the derivative gain K_d and it is given by:

$$D_{out} = K_d \frac{d}{dt} e(t) \qquad (2.3)$$

Where, D_{out} is the derivative term of output.

The derivative action of PID controller can amplify the noise and reflected it as chatter in the controller output signal. So in some applications we implement an external filter at the output of PID controller. But the filter can introduce a delay in the system.

The output of PID controller is defined as u(t), the final form of the PID algorithm is:

$$u(t) = K_p e(t) + K_i \int_0^t e(\tau)d\tau + K_d \frac{d}{dt} e(t) \qquad (2.4)$$

The weighted sum of these three actions is used to adjust the process via a control element such as the position of the rotor in this thesis. By tuning these three constants in the PID controller algorithm, the controller can provide control action designed for specific process requirements.

The advantages of PID controller:

- High level of practicability due to intuitive and physical motivated design process.
- Easily extendable by "hand-made" structural enhancements.
- Well suited for SISO control schemes.

The disadvantages of PID controller:

- As soon as industrial active magnetic bearing systems becoming more complex, the PID control might become less important in such systems in the future.
- The use of the PID algorithm for control does not guarantee optimal control of the system or system stability.

This thesis started from PID controller to design the control system. And then, that will be analyzed in detail in chapter 4.

2.2.2 H-infinity Control

H-infinity control theory approaches the problem from the point view of classical sensitivity theory. The basic problem of H-infinity theory is reducing sensitivity of feedback control systems and then achieves robust performance or stabilization. The technique is concerned with the effects of feedback on uncertainty, where the uncertainty may be in the form of an additive disturbance U(s) as illustrated in figure2.6.

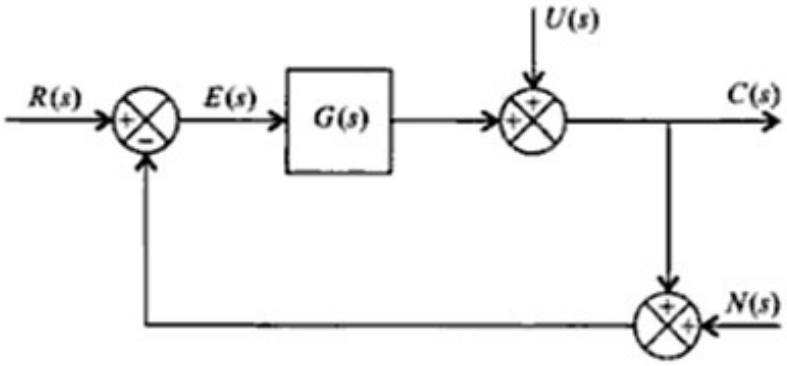

Figure 2.6 Control system containing a disturbance and noise

The controller of H-infinity is designed by frequency domain weighting functions. H-infinity control theory attempts to minimize the supreme function over the entire frequency range

$$u = \sup_{w} \left| S(jw) W(jw) \right| \qquad (2.5)$$

Where, $S(j\omega)$ is the sensitivity function and $W(j\omega)$ is a weighting function. The weighting function emphasizes that low sensitivity is more important at low frequency than higher frequency. Therefore, the weighting function is greatest at those frequencies where the sensitivity is the smallest - namely at low frequencies [4].

The advantages of H-infinity technique:

- Practical choice of weighting functions based on engineering specifications.
- High robustness to plant and uncertainties.
- Highly suited for complex plants and MIMO control problems.
- It has a high technical potential for industrial applications.

On the contrary, this technique still rarely used and controller order requires large computational resources (digital control).

2.2.3 Suggestion of Another Control Algorithm

Depending on the high maintenance, the wind turbines need to be more robust. Therefore, we can use the wind turbines as long as possible and also save the costs. However, the intense non-linear and uncertainty of parameters of the magnetic bearings make the traditional PID controller difficult to ensure its long-term and stable operation. So, robust control is concerned with determining a stabilizing controller that achieves feedback performance in terms of stability and accuracy requirements.

As mentioned in chapter 2, except PID control method, the most important state-of-the-art control design method for AMB system is H-infinity control. Compare these two control algorithms in table 6-1.

Table 6-1 Compare of PID controller and H-infinity control

Method	Advantages	Drawbacks
PID controller	• High level of practicability due to intuitive and physical motivated design process. • Easily extendable by "hand-made" structural enhancements. • Well suited for SISO control schemes	• As soon as industrial active magnetic bearing systems becoming more complex, the PID control might become less important in the future. • The use of the PID algorithm for control does not guarantee optimal control of the system or system stability.
H-infinity control	• Practical choice of weighting functions based on engineering specifications. • High robustness to plant and uncertainties. • Highly suited for complex plants and MIMO control problems. • Have a high technical potential for industrial applications.	• High controller order requires large computational resources (digital control)

As shown in table 6-1, H-infinity control is more robustness to plant and uncertainties. Therefore, we introduce a method, which is based on quantitative feedback theory (QFT) and H-infinity control theory, to solve this problem.

QFT and H-infinity control both are the design method of robust controller for uncertainty controlled plant. The structure of QFT is shown in figure 6.1. [21]

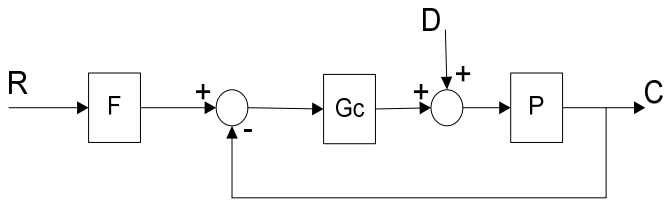

Figure 6.1 Structure of QFT [21]

From [22] and [23], the design objective is to design the prefilter F(s) and the compensator G(s), so the robust control design is satisfied for the requirements of the system. The design procedure to accomplish this objective is as follow:

1) According to the requirements, the closed-loop transfer function of system should be satisfied by equation (6.1)

$$\left|T_l(j\omega)\right| \le \left|T_b(j\omega)\right| \le \left|T_u(j\omega)\right| \quad (6.1)$$

Where, $T_l(w)$ and $T_u(w)$ are respectively the lower bound function and upper bound function of the closed-loop system on frequency domain. If the current stiffness and displacement stiffness vary in allowable range of the control system, and all the response curves of closed-loop transfer function $T_b(s)$ in frequency domain locate between upper and lower boundary. Therefore, the dynamic performance of the system is satisfied.

2) As shown in figure 6.2, the prefilter F(s) in figure 6.1 is removed, and the weight function is introduced to the system main controller $G_c(s)$. The main controller $G_c(s)$ is solved based on H-infinity control theory.

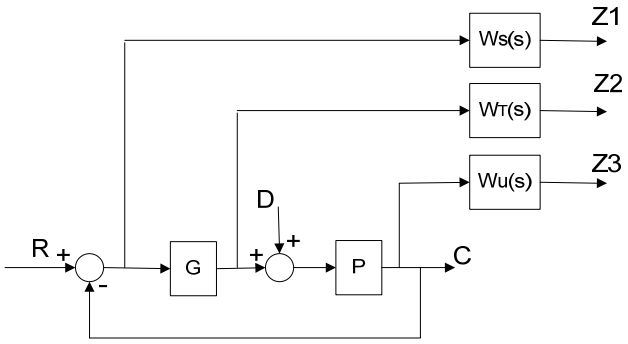

Figure 6.2 Control system with weight functions

3) After designing the main controller G(s), the filter F(s) is added into the closed-loop system to modify the control performance, which to make sure the closed-loop transfer function $T_b(s)$ satisfied equation (6.1).

As discussed before, the transfer function of magnetic bearing is

$$P(s) = \frac{k_i}{ms^2 - k_x} \quad (6.2)$$

The upper and lower boundary transfer function of QFT is expressed in

$$G(s) = \frac{\omega_n^{\,2}}{s^2 + 2\xi\omega_n s + \omega_n^{\,2}} \quad (6.3)$$

Where, ξ and ω_n are the damping coefficient and the natural oscillation frequency respectively.

The upper boundary belongs to under-damping situation, so $0 < \xi < 1$. Therefore, the overshoot and settling time of the system need to be satisfied to the following equations. [23]

The overshoot of the system is:

$$\sigma = e^{-\pi\xi/\sqrt{1-\xi^2}} \times 100\% \tag{6.4}$$

The settling time of the system is:

$$t_s \approx \begin{cases} 3.2/(\varsigma\omega_n) \\ \dfrac{2.8 + 6.5(\xi - 0.7)}{\omega_n} \end{cases} \tag{6.5}$$

The lower boundary belongs to over-damping situation, the system has no overshoot, and the regulating time is shown as

$$t_s \approx (6.45\xi - 1.7)/\omega_n \tag{6.6}$$

Depending on the requirement of the system performance, determine the value of ξ and ω. With the value of coefficients ξ and ω. Calculate the upper and lower bound function $T_u(s)$ and $T_l(s)$.

As discussed before, the controller is designed based on H-infinity control theory and the solving process of controller is usually transformed into the standard design problem. The choice of the weighting functions is shown below. [22]

a) $W_s(s)$ is used to limit the sensitivity function S(s), and ensure the performance index of the closed-loop system achieved the requirement. W(s) must satisfy

$$\left|W_s(j\omega)S(j\omega)\right| \le 1. \tag{6.7}$$

b) $W_T(s)$ is used to limit the complementary sensitivity function T(s) and ensure the system stable when the system exist uncertainty. $W_T(s)$ is satisfied by

$$\left|P(j\omega)/P_0(j\omega) - 1\right| \le \left|W_T(j\omega)\right| \tag{6.8}$$

c) $W_u(s)$ is used to restrain the sensor noise and high frequency disturbance, and mainly consider the transfer function $T_{un}(s)$. The $W_u(s)$ is satisfied by

$$\left|W_u(j\omega)T_{un}(j\omega)\right| \le 1 \tag{6.9}$$

After determine the weighting functions, the predicting filter F(s) is added into the system. With Matlab/Simulink, modified F(s) to guarantee all the response curves of the closed-loop system are in the upper and lower boundary.

Therefore, the designed QFT-H-infinity magnetic bearing controller can ensure the system to have high performance when there are the changes in model parameters and external disturbances. It can improve the reliability and stability of the magnetic bearings system.

2.2.4 Other Control Methods

Here, table 2.1 gives an overview of the control design methods that are well-known but not widely used for active magnetic bearing systems. In the table, the descriptions are starting with "•", the advantages are starting with "+", and the disadvantages are starting with "-".

Table 2.1 well-known but rarely applied control design methods for AMB systems [5]

method	short description and validation
pole-placement	• full order state feedback • direct prescription of closed-loop system dynamics - requires all system states to be measurable - sensible choice of closed-loop system poles requires high skillfulness - bandwidth limitations and sensor noise difficult to address
LQ-control	• full order state feedback • "L"--linear, "Q"--quadratic • minimization of a quadratic cost function - requires all system states to be measurable - requires skill and experience for proper choice of weighting matrices + bandwidth limitations manageable by weighting matrices
LQG-control	• output feedback (not all states must be measurable) • "L"--linear, "Q"--quadratic, "G"--Gaussian • minimization of a quadratic cost function + estimation of non-measurable system states by linear full order state observer scheme - requires skill and experience for proper choice of weighting matrices - requires exact knowledge of plant dynamics
structure predefined control	• output feedback • allows to apply LQ-control design methodology without necessity for implementing a full order observer + arbitrary controller structure pre-definable - requires skill and experience for proper choice of weighting matrices - low robustness to plant uncertainties

Chapter 3 Model of the MB System

In this chapter, the actuator model and the model of rotation rigid rotor without gyroscopic effect is discussed first. Linear mode of the actuator is described in section 3.1 and the dimensions of actuators in this thesis are shown in the end. And later, section 3.2 combines the rotor and actuator model. Then the model of the magnetic bearing system is given. Moreover, the gyroscopic effect in this system is considered.

3.1 Actuator Model

The electromagnetic type magnetic bearings exert forces on the rotor without direct physical contact. The forces can be generated from the currents in the electromagnet coils.

3.1.1 Magnetic bearing force

The actuator is designed in "U" core with a group of ferromagnetic metal discs, and the surface area of the tooth is defined in A.

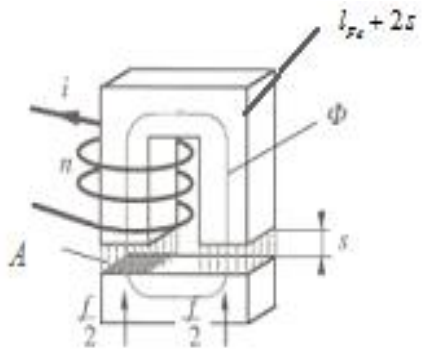

Figure 3.1 a simple magnetic circuit

A simple magnetic circuit is shown in figure 3.1. Using Ampere's Law,

$$\oint Hds = H_{fe}l_{fe} + H_g 2s = ni \tag{3.1}$$

$$l_{fe}\frac{B_{fe}}{\mu_0\mu_r} + 2s\frac{B_g}{\mu_0} = ni \tag{3.2}$$

In this thesis, the surface area of the teeth is not designed in flat as shown in figure 3.1, but designed in an arc such as the rotor surface as shown in figure 3.2. Therefore, it assumes that all the flux passes through the teeth perpendicularly so that the surface area of the air gap is equal to the surface area of the tooth. Then

$$\phi = B_{fe} A_{fe} = B_g A_g$$
$$A_{fe} = A_g \tag{3.3}$$
$$B = B_{fe} = B_g$$

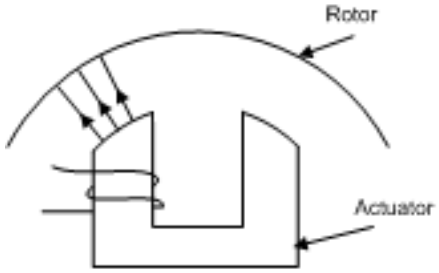

Figure 3.2 Assumption of actuator surface

Therefore,

$$B = \mu_0 \frac{ni}{\frac{l_{fe}}{\mu_r} + 2s} \tag{3.4}$$

Where

μ_0 is the magnetic permeability in the air;

μ_r is the relative magnetic permeability of the steel;

s is the air gap length;

l_{fe} is the magnet length;

n is the number of coils.

In most cases, the permeability of the steel material is taken to be infinite even though that is not the case in reality. However the permeability of steel is much higher than the air. So assume that the energy will be stored in the air gap. Then the equation (3.4) can be written as

$$B = \frac{ni}{2s} \mu_0 \tag{3.5}$$

The magnetic energy stored in the air gap is given by

$$W = \frac{1}{2} \int_v BHdV = \frac{1}{2} B_g H_g 2sA_g \tag{3.6}$$

Using the principle of virtual displacement

$$F = \frac{\partial W}{\partial s} = B_g H_g A_g = \frac{B_g^2}{\mu_0} A_g \qquad (3.7)$$

Replacing the value of B in this equation

$$F = \mu_0 \frac{1}{4} n^2 A \frac{i^2}{s^2} = k \frac{i^2}{s^2} \qquad (3.8)$$

Where $k = \frac{1}{4} \mu_0 n^2 A$

The change in forces due to the change in current or the air gap is a quadratic function that is non-linear. In control theory, linear relations are preferred, because control of a linear system is much easier than a nonlinear system. This equation can be linearized about a certain operation point of the current and the air gap.

3.1.2 Linearization of magnetic bearings

Magnetic bearings are mostly used in differential driving mode. This configuration makes it possible to generate both positive and negative forces. The geometry is shown in figure 3.3. The figure shows a differential mode of operation to levitate 1 degree of freedom of the mass m. In this case, the operating points for the magnetic bearing are at i_0, which is also called the bias current and a position s_0. One magnet is driven with the sum of bias current i_0 and control current i_x, and the other one with the difference i_0-i_x. The increase in current means increase the attractive force in windings and vive versa. When the rotor displaces a distance x from the operating position, the force in the corresponding air gap increases and the force in opposite air gap decreases. And then, to bring the rotor back to the original position, the current in the larger gap side should be increased which means the current in the opposite will be decreased.

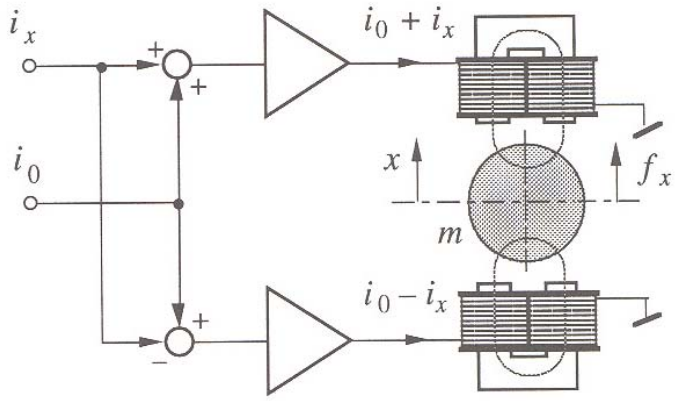

Figure 3.3 A differential driving mode of magnetic bearings

The total force acting in that axis is

$$f_x = f_+ - f_- = k\left(\frac{(i_o + i_x)^2}{(s_0 - x)^2} - \frac{(i_0 - i_x)^2}{(s_0 + x)^2}\right) \tag{3.9}$$

Where, $k = \frac{1}{4}\mu_0 n^2 A_g$ (3.10)

If simplify and linearize eq. (3.9) with respect to x « s_0, the equation then can be given by

$$f_x = \underbrace{\left(\frac{4ki_0}{s_o^2}\right)}_{k_i} i_x + \underbrace{\left(\frac{4ki_0^2}{s_0^3}\right)}_{k_x} x \tag{3.11}$$

Then it can be written as

$$f_x = k_i i_x + k_x x \tag{3.12}$$

In which k_i is called force/current factor and k_x is called force/displacement factor. And they can be described in

$$k_i = \frac{4ki_0}{s_0^2} \tag{3.13}$$

$$k_x = \frac{4ki_0^2}{s_0^3} \tag{3.14}$$

3.1.3 Dimensions of actuators

In this thesis, we have radial actuators and axial actuators. They are all designed in U-core type as shown below:

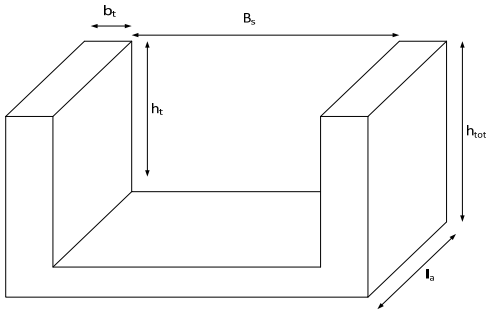

Figure 3.4 Drawing of actuator

And the data of radial actuator and axial actuator are shown in table 1 and table 2.

Table 3-1 Dimensions of the radial actuator

Radial Actuator Design	Nominal	Maximum
Design flux density	0.72T	1T
Air gap change	0.5mm	1mm
Air gap	1.5mm	2.5mm
Force (estimated)	288N	557N
Number of turns	390	390
Width of tooth (bt)	10mm	10mm
Length of tooth (la)	70mm	70mm
Slot width (bs)	40mm	40mm
Height of tooth (ht)	60mm	60mm
Height of actuator (htot)	70mm	70mm
Fill factor	0.3	0.3
Current density	$3.2A/mm^2$	$6A/mm^2$
Radius of wire	0.65mm	0.65mm
Current	6A	6A
Length of conductor	101m	101m
Mass of copper (per act.)	0.9kg	0.9kg
Mass of iron (per act.)	0.9kg	0.9kg
Total mass per act	1.8kg	1.8kg
Loss bias $\alpha = 0.5$ (per actuator)	20W	-
Loss total (per actuator)	81W	225W
Resistance of the coil (90 degrees)	2.25ohms	2.25ohms
Inductance of the coil	91.4mH	64.4mH

Table 3-2 Dimension of axial actuator

Axial actuator design	Nominal	Maximum
Design flux density	0.3T	0.37T
Air gap change	0.5mm	1mm
Air gap	1.5mm	2.5mm
Force	18.35N	26N
Number of turns	200	200
Width of tooth (bt)	12mm	12mm
Length of tooth (la)	20mm	20mm
Slot width (bs)	20mm	20mm
Height of tooth (ht)	32.5mm	32.5mm
Height of actuator (htot)	38.5mm	38.5mm
Fill factor	0.3	0.3
Current density	$4A/mm^2$	$7.5A/mm^2$
Radius of wire	0.55mm	0.55mm
Current	3.7A	7.3A
Length of conductor	26m	26m

Mass of copper (per act.)	0.22kg	0.22kg
Mass of iron (per act.)	0.2kg	0.2kg
Total mass per act	0.42kg	0.42kg
Loss bias	2W	-
Loss total (per actuator)	8W	30W
Resistance of the coil (90 degrees)	0.6ohms	0.6ohms
Inductance of the coil	5.9mH	3.9mH

3.2 Rotor and Actuator Models

This section followed the reference [5], which is talking about a spindle rotor with magnetic bearings.

Figure 3.5 displays the model of rigid rotor with actuators and position sensors. In this system, there are two pairs of radial actuators and four pairs of axial actuators. And the actuators are in differential mode which has been introduced in last section. The position sensors are also shown in the picture, and two more sensors are shown on the other side of the rotor.

For modeling the rotor, there are some assumptions need to be considered first:

- The rotor is symmetric and rigid.
- The axial actuator can be treated separately and independently from the radial one.
- Because the diameter of the rotor is big, the air gap of magnetic bearing is considered as a flat plate.
- Sensor and magnet are in the same position.

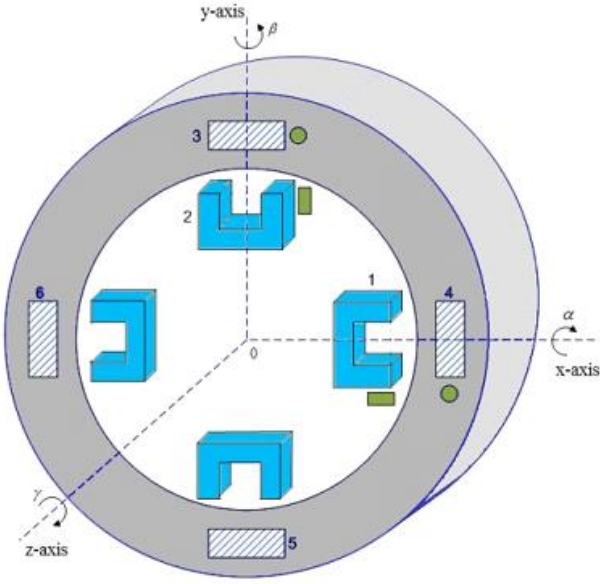

Figure 3.5 The rigid rotor with actuator and position sensors

3.2.1 Mathematical modeling

As shown in figure 3.4, six pairs of actuators and related sensors are given in numbers 1 to 6 separately. This thesis discusses the rotor in five degree of freedoms. According to figure 3.6 generalized coordinates are used. The air gap displacements x, y, z on the three dimensions and related angles α, β, γ all combined into the vector p described in equation (3.15). The rotor speed is Ω, and the spin velocity $\dot{\gamma} = \Omega$ is assumed to be a constant. The measured air gap displacements x_1, x_2, x_3, x_4, x_5, and x_6 are comprised in vector q described in (3.16). The individual coil control currents of all magnetic bearings described in equation (3.17)

$$\mathbf{p} = \begin{bmatrix} x \\ y \\ z \\ -\alpha \\ \beta \end{bmatrix} \tag{3.15}$$

$$\mathbf{q} = \begin{bmatrix} x_1 \\ x_2 \\ x_3 \\ x_4 \\ x_5 \\ x_6 \end{bmatrix} \tag{3.16}$$

$$\mathbf{i} = \begin{bmatrix} i_1 \\ i_2 \\ i_3 \\ i_4 \\ i_5 \\ i_6 \end{bmatrix} \tag{3.17}$$

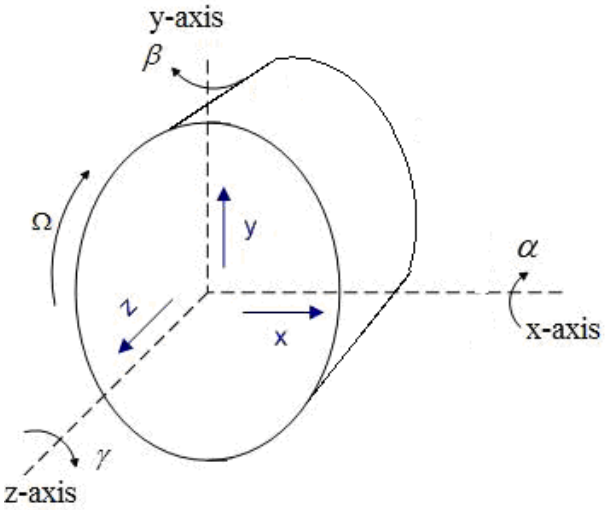

Figure 3.6 Coordinate directions of rotor

The forces u_f of magnetic bearings is expressed in (3.18). In the last section, the magnetic bearing force u_f can be described as a linearized function of the rotor displacements in the bearing and the coil currents, involving the force/current factor k_i and the force/displacement factor k_x. In general, these constant factors of radial actuators and axial actuators are not the same; however, these factors can be described with subscripts. k_{i1} & k_{x1} are for radial actuators, and k_{i2} & k_{x2} are for axial actuators.

$$\mathbf{u}_f = \begin{bmatrix} f_1 \\ f_2 \\ f_3 \\ f_4 \\ f_5 \\ f_6 \end{bmatrix} = \mathbf{k}_x\mathbf{q} + \mathbf{k}_i\mathbf{i} \tag{3.18}$$

To simplify the rotor model, the gyroscopic effect is not considered in this part. From Newton's Law, the equation of motion for the setup of figure 3.4 is shown following:

$$\mathbf{M}\ddot{\mathbf{p}} = \mathbf{u}_f \tag{3.19}$$

$$\mathbf{M}\ddot{\mathbf{p}} = \mathbf{k}_x\mathbf{q} + \mathbf{k}_i\mathbf{i} \tag{3.20}$$

The vector M is the diagonal mass matrix as shown in equation (3.21). Vector **f** describes the forces of all magnetic bearings, as a function of control currents describes by vector **i** and the bearing coordinates **q**.

The rotor rotates in six degree of freedoms (dofs). As shown in figure 3.6, these six degree of freedoms are move left-right, move up-down, translation along z-axis, rotation around x-axis,

rotation around y-axis, and rotation around z-axis. Among them, rotation around z-axis is normal situation. When the rotor rotates in the other five dofs, the actuators are in different conditions. The radial and axial actuators have been named with number 1 to 6 as shown in figure 3.3.

- If the rotor moves left-right, the radial actuator number 1 act. So the force on the rotor is $f=f_1$.
- If the rotor moves up-down, only radial actuator number 2 act. Hence the rotor on the rotor is $f=f_2$.
- If the rotor translation along z-axis, all the axial actuators take the rotor back to the original position. So number 3, 4, 5, and 6 actuators are act. Here, the force on the rotor is $f=f_3=f_4=f_5=f_6$.
- If the rotor rotation around x-axis, axial actuators 3 and 5 act. The force on the rotor of 3 and 5 are opposite. Hence, the torque f*r is equal to f_3*r +f_5*r. We assume the force of actuators 3 and 5 are the same, and they are half of the force act on the rotor.
- If the rotor rotation around y-axis, axial actuators 4 and 6 act. The situation is as the same as the rotor rotation around x-axis. So the force of actuator 4 and 6 are half of the force act on the rotor.

Then the equation (3.20) can be written as

$$\begin{bmatrix} m & 0 & 0 & 0 & 0 \\ 0 & m & 0 & 0 & 0 \\ 0 & 0 & m & 0 & 0 \\ 0 & 0 & 0 & I_x & 0 \\ 0 & 0 & 0 & 0 & I_y \end{bmatrix} \begin{bmatrix} \ddot{x}_1 \\ \ddot{x}_2 \\ \ddot{x}_3 \\ \ddot{x}_4 \\ \ddot{x}_5 \\ \ddot{x}_6 \end{bmatrix} = \begin{bmatrix} k_{x1} & 0 & 0 & 0 & 0 & 0 \\ 0 & k_{x1} & 0 & 0 & 0 & 0 \\ 0 & 0 & k_{x2} & k_{x2} & k_{x2} & k_{x2} \\ 0 & 0 & k_{x2}r & 0 & -k_{x2}r & 0 \\ 0 & 0 & 0 & k_{x2}r & 0 & -k_{x2}r \end{bmatrix} \begin{bmatrix} x_1 \\ x_2 \\ x_3 \\ x_4 \\ x_5 \\ x_6 \end{bmatrix} + \begin{bmatrix} k_{i1} & 0 & 0 & 0 & 0 & 0 \\ 0 & k_{i1} & 0 & 0 & 0 & 0 \\ 0 & 0 & k_{i2} & k_{i2} & k_{i2} & k_{i2} \\ 0 & 0 & k_{i2}r & 0 & -k_{i2}r & 0 \\ 0 & 0 & 0 & k_{i2}r & 0 & -k_{i2}r \end{bmatrix} \begin{bmatrix} i_1 \\ i_2 \\ i_3 \\ i_4 \\ i_5 \\ i_6 \end{bmatrix} \tag{3.21}$$

In the expression (3.21), $I_x = I_y = mr^2$ are the moments of inertia respect to axis x and y. Where, r is the radius of the rigid rotor.

In order to discuss the properties of the resulting closed-loop system it is essential to involve only one set of coordinates for the motion description. This can be easily achieved by transforming **p** into **q** by means of a linear transformation matrix $\mathbf{T_s}$ as shown below

$$\mathbf{p}=\begin{bmatrix} x \\ y \\ z \\ -\alpha \\ \beta \end{bmatrix}=\begin{bmatrix} 1 & 0 & 0 & 0 & 0 & 0 \\ 0 & 1 & 0 & 0 & 0 & 0 \\ 0 & 0 & 1/4 & 1/4 & 1/4 & 1/4 \\ 0 & 0 & -1/2r & 0 & 1/2r & 0 \\ 0 & 0 & 0 & 1/2r & 0 & -1/2r \end{bmatrix}\begin{bmatrix} x_1 \\ x_2 \\ x_3 \\ x_4 \\ x_5 \\ x_6 \end{bmatrix}=\mathbf{T}_s\mathbf{q} \tag{3.22}$$

Where, $\mathbf{T}_s=\begin{bmatrix} 1 & 0 & 0 & 0 & 0 & 0 \\ 0 & 1 & 0 & 0 & 0 & 0 \\ 0 & 0 & 1/4 & 1/4 & 1/4 & 1/4 \\ 0 & 0 & -1/2r & 0 & 1/2r & 0 \\ 0 & 0 & 0 & 1/2r & 0 & -1/2r \end{bmatrix}$

Insert $\mathbf{T}_s$ into (3.21), it can be written as

$$\begin{bmatrix} m & 0 & 0 & 0 & 0 & 0 \\ 0 & m & 0 & 0 & 0 & 0 \\ 0 & 0 & 1/4m & 1/4m & 1/4m & 1/4m \\ 0 & 0 & -I_x/2r & 0 & I_x/2r & 0 \\ 0 & 0 & 0 & I_y/2r & 0 & -I_y/2r \end{bmatrix}\begin{bmatrix} \ddot{x}_1 \\ \ddot{x}_2 \\ \ddot{x}_3 \\ \ddot{x}_4 \\ \ddot{x}_5 \\ \ddot{x}_6 \end{bmatrix}$$

$$=\begin{bmatrix} k_{x1} & 0 & 0 & 0 & 0 & 0 \\ 0 & k_{x1} & 0 & 0 & 0 & 0 \\ 0 & 0 & k_{x2} & k_{x2} & k_{x2} & k_{x2} \\ 0 & 0 & \frac{1}{2}k_{x2}r & 0 & -\frac{1}{2}k_{x2}r & 0 \\ 0 & 0 & 0 & \frac{1}{2}k_{x2}r & 0 & -\frac{1}{2}k_{x2}r \end{bmatrix}\begin{bmatrix} x_1 \\ x_2 \\ x_3 \\ x_4 \\ x_5 \\ x_6 \end{bmatrix}+\begin{bmatrix} k_{i1} & 0 & 0 & 0 & 0 & 0 \\ 0 & k_{i1} & 0 & 0 & 0 & 0 \\ 0 & 0 & k_{i2} & k_{i2} & k_{i2} & k_{i2} \\ 0 & 0 & \frac{1}{2}k_{i2}r & 0 & -\frac{1}{2}k_{i2}r & 0 \\ 0 & 0 & 0 & \frac{1}{2}k_{i2}r & 0 & -\frac{1}{2}k_{i2}r \end{bmatrix}\begin{bmatrix} i_1 \\ i_2 \\ i_3 \\ i_4 \\ i_5 \\ i_6 \end{bmatrix} \tag{3.23}$$

Therefore, $\mathbf{M}\ddot{\mathbf{q}}=\mathbf{k}_{xs}\mathbf{q}+\mathbf{k}_i\mathbf{i}$ (3.24)

Taking Laplace transform of the modeling equation (3.24)

$$\mathbf{M}s^2\mathbf{q}(\mathbf{s})-\mathbf{k}_{xs}\mathbf{q}(\mathbf{s})=\mathbf{k}_i\mathbf{i}(\mathbf{s}) \tag{3.25}$$

Where, $\mathbf{i(s)}$ is the input of the system.

The transfer function between output and input,

$$\mathbf{q(s)} = (\mathbf{M}s^2 - \mathbf{k_{xs}})^{-1}\mathbf{k_i i(s)} \tag{3.26}$$

3.2.2 Gyroscopic effect

When apply a force on a rotation rotor, acting during a very short time, is leading to a change in direction for the axis of the moment of momentum. This is called gyroscopic effect. When considering gyroscopic effect in this system, the form (3.20) can be described in

$$\mathbf{M}\ddot{\mathbf{q}} + \mathbf{G}\dot{\mathbf{q}} = \mathbf{k}_{xs}\mathbf{q} + \mathbf{k}_i\mathbf{i} \tag{3.27}$$

The gyroscopic effects are typically characterized by a skew-symmetric matrix,

$$\mathbf{G} = \begin{bmatrix} 0 & 0 & 0 & 0 & 0 \\ 0 & 0 & 0 & 0 & 0 \\ 0 & 0 & 0 & 0 & 0 \\ 0 & 0 & 0 & 0 & -1 \\ 0 & 0 & 0 & 1 & 0 \end{bmatrix} I_z\Omega \tag{3.28}$$

In this system, $I_z = mr^2$ is the moment of inertia to z-axis.

Gyroscopic effect always considered in high speed condition. But in this system, the speed is not too high. Therefore the gyroscopic effect is not considered first.

Chapter 4 Control System Design

In the previous chapters, a model of rotor and actuator has been designed. This model needs a control system, which includes electronic circuits and digital control design. Section 4.1 talks about the electronic circuits used to measure the signal in this system. That can be divided into two main parts: one is from sensor output to DSP, the other one is from DSP output to amplifiers. Later, a proper control algorithm is addressed to this project in section 4.2. Based on that, the control circuit is designed for this algorithm, and then, implemented the control algorithm into the controller. In the last section, decentralized control is discussed and compared with central control.

4.1 Electronic Circuit Design

In the system design, the completed structure of the magnetic bearing demonstrator is shown in figure 4.1. From this overview of the system, there are two main parts of the electronic circuit. One is power supply + Signal conditioning, and the other one is isolation.

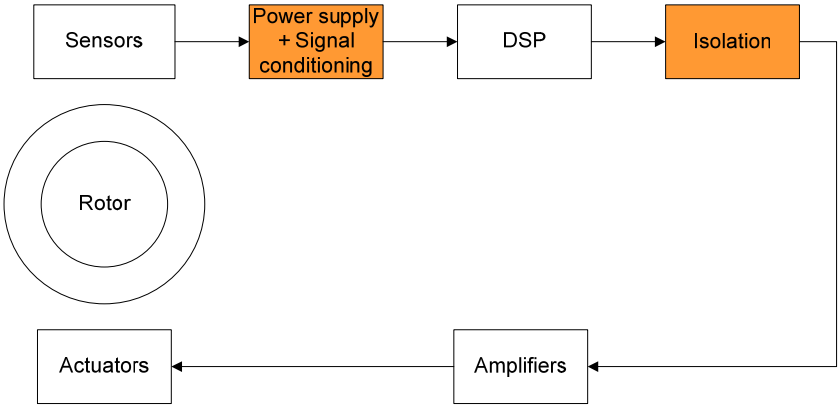

Figure 4.1 Block design of the whole system

4.1.1 Two Boards Layout

The electronic circuit of this system can be divided into two boards. The first one is called sensor output board, and the other one is called DSP output board. The layouts of these two boards are shown in figure 4.2 (a) and (b).

In board one, there are 12 pins input to the board from six sensors output. On the other side, 7 pins output to DSP controller. Moreover, there is a voltage regulator support 24dc voltage to board two.

In board two, there are 24 pins input from DSP output, and through opto coupler get the isolated PWM signals to 12 amplifiers.

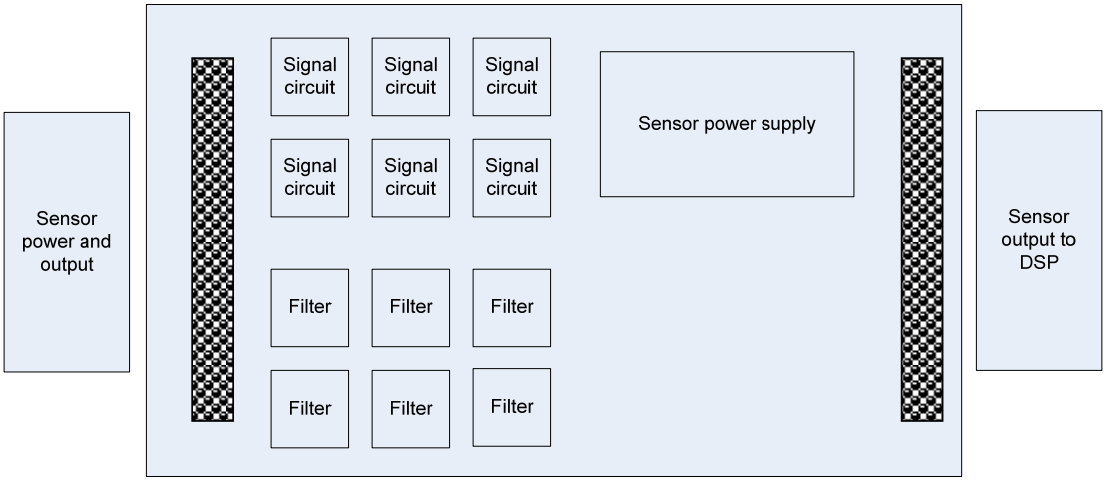

(a)

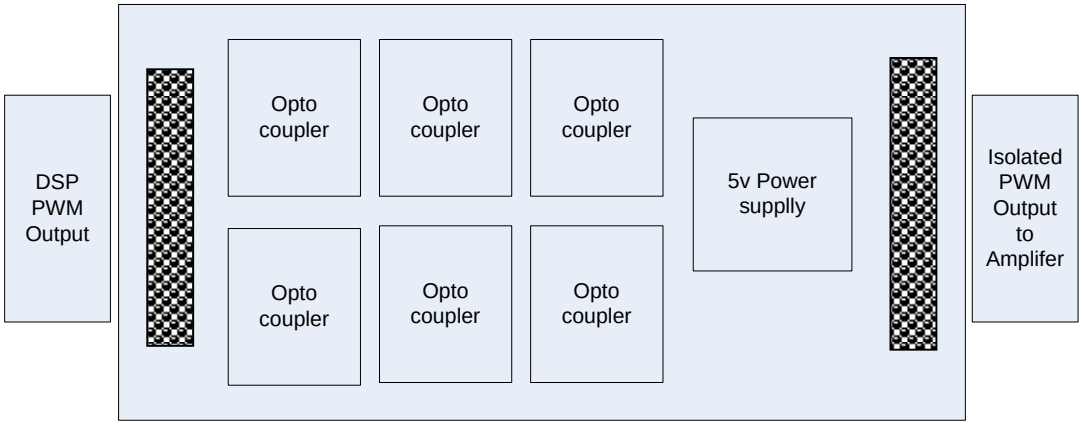

(b)

Figure 4.2 (a) Sensor output board (b) DSP output board

In these two boards, there are a lot of components are used. Table 4-1 shows the types of these components.

Table 4-1 the list of components

Name	Type
Op-amp	LM124A
Opto coupler	HCPL 2219/2200
DC-DC converter	NMH Series Isolated 2W dual output dc-dc converter
Voltage regulator	L7800 Series
Bridge rectifier	FL400 Series

4.1.2 Circuit Design

4.1.2.1 Signal Circuit

As shown in figure 4.2 (a), the signal conditioning circuit section is used to transfer the sensor output signal to DSP controller. In this project, the signal of sensor output is from 0V to 10V. However, the maximum ADC signal input of DSP is 3.0V. So the signal circuit is needed to transfer 10V to 3V as maximum.

To solve this problem, two resistances are used as voltage transformation. Figure 4.3 shows the drawing of signal circuit and the value of resistances.

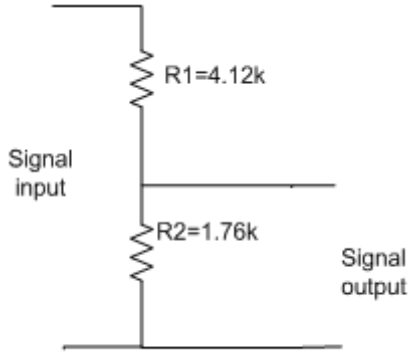

Figure 4.3 Signal circuit drawing

4.1.2.2 Isolation components

An opto coupler used to get an isolated PWM signal, and then, input to 12 amplifiers. Here, a dual-in-line package with 8pins opto coupler is used. So, each this kind of opto coupler can handle 2 different signals. Therefore, six opto couplers are used in this project. Moreover, this type of opto coupler needs 5V power supply.

4.1.2.3 Power Supply

The power input to this system is 24AC voltage. But for different elements, the power supplies are different. However, the electronic circuits are needed to support power supplies to each part of the system.

1. ***24dc voltage for sensor power supply.***

This part is designed with a bridge rectifier and two voltage regulators. The bridge rectifier is used for conversion of an alternative current (AC) input into a direct current output (DC). Voltage regulator of the system is able to provide a constant voltage over a wide range.

A 24VAC input to this board is transferred from 220VAC by a transformer out of the board. The power supply of the sensor in this system needs 24VDC and 205mA. Bridge rectifier and voltage regulators are used to transfer 24VAC to 24VDC to the sensor. The voltage regulator, which used

in this system, can only support 150mA current for each one. So, two voltage regulators are designed together to provide the current to the sensor. The schematic of this sensor power supply is shown in figure 4.4.

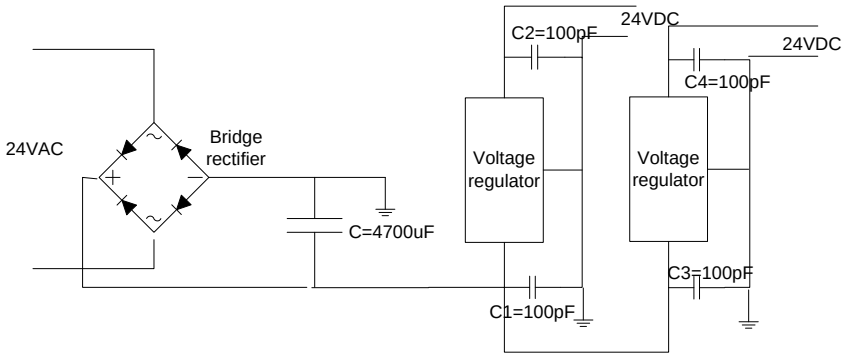

Figure 4.4 Schematic of power supply for sensor

2. 15dc voltage for op-amp power supply

In sensor output board, op-amp needs $\pm 15V$ power supply. In this system another voltage regulator connected from the bridge rectifier to a dc-dc converter, and then, gets a 15VDC to op-amp power supply. The 24VDC output from voltage regulator will be the input to the DSP output board. The drawing of this part is shown below.

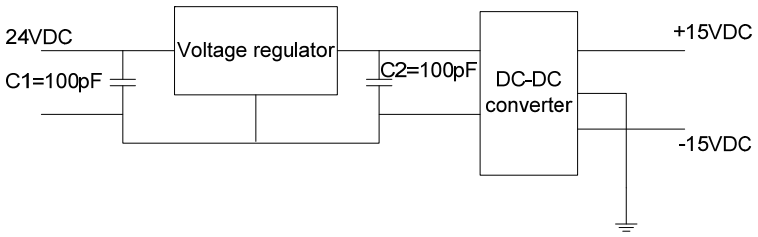

Figure 4.5 Schematic of op-amp power supply

3. 5dc voltage for opto coupler power supply

A 24VDC input from the sensor output board, can be transferred into 5VDC by a dc-dc converter. The schematic is shown as

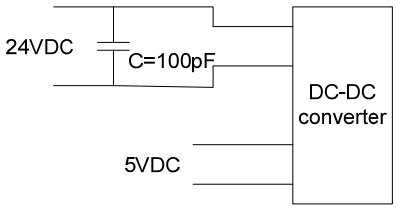

Figure 4.6 Schematic of opto coupler power supply

4.1.2.4 Filter Design

A filter is a device that passes electric signals at certain frequencies or frequency ranges while preventing the passage of others. — Webster. [16]

A filter can be either in active or passive. Here, an active filter is used in this thesis, because it is much cheaper and simple than a passive filter. Active filters are circuits that use an operational amplifier (op-amp) as an active device with some resistors and capacitors. In this project, a type of dual-in-line package with 14 pins is used. So, this kind of op-amp can deal with 4 different signals. Therefore, only two op-amps are needed in this project.

A higher order filter will induce more delay to the system, and this system needs fast response. Therefore, in our design, a second order filter is required. A Bessel filter exhibits a nearly constant time delay to frequencies within the pass band. If the phase increases nearly with frequency, its effect is simply to delay the output signal by a constant time period. However, if the phase shift is not directly proportional to frequency, it can present problems. So in our design, a second order Bessel filter is designed. The schematic of a 2nd order Bessel filter is shown in figure 4.7.

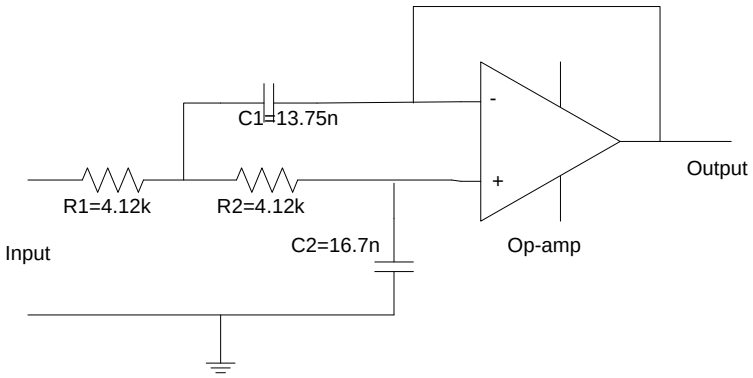

Figure 4.7 Schematic of 2nd order Bessel filter

It is assumed that the system frequency is lower than 2 kHz. So we estimate the cut-off frequency is 2 kHz.

The transfer function of Bessel filter is expressed in:

$$G(s) = \frac{K_0}{Be_n(\frac{s}{\omega_0})} \tag{4.1}$$

Where, K_0 is chosen such that the dc gain is 1.

ω_0 is chosen such that the desired cut-off frequency ω_c is obtained.

$Be_n(s)$ is a Bessel polynomial generated as follow table:

Table 4-2 Bessel polynomial [18]

n	$Be_n(s)$	K_0
1	1+s	1
2	$3+3s+s^2$	3
3	$15+15s+6s^2+s^3$	15

The transfer function of figure 4.7 is $G(s) = \dfrac{1}{1+\omega_c C_2(R_1+R_2)s+\omega_c{}^2 R_1 R_2 C_1 C_2 s^2}$

As discussed before, the cutoff frequency is limited in 2 kHz. According to the table 4-2, and adjusting the values of components in Multisim, the parameters of Bessel filter is shown in table 4-3.

Table 4-3 parameters of designed filter

Parameters	R_1	R_2	C_1	C_2
Values	4.12kohm	4.12kohm	13.75nf	16.7nf

Moreover, the bode plot of this Bessel filter is shown in figure 4.8. From the diagram, the cut-off frequency is limited in 2 kHz.

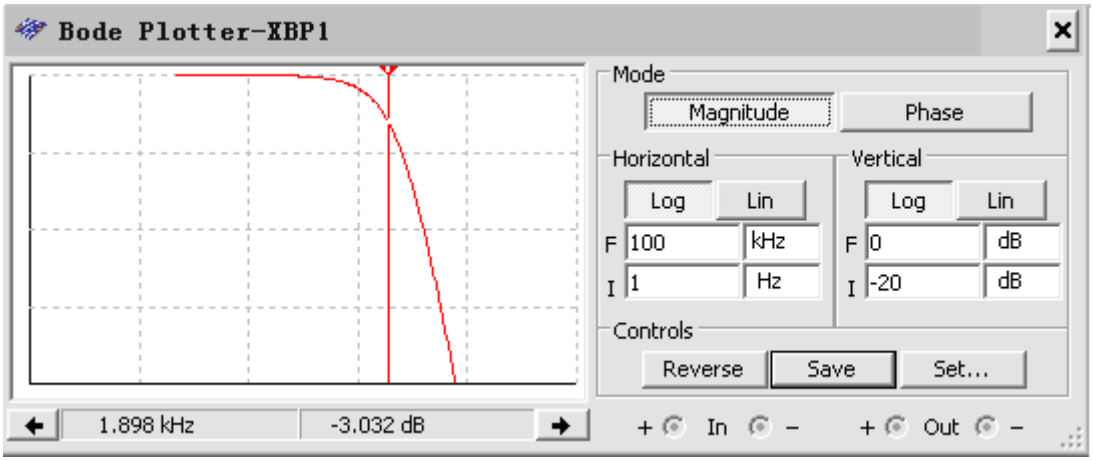

Figure 4.8 Bode plot of Bessel filter

4.2 Control Design

This thesis interests in PID controller and decentralized control, which means the system is controlled in 5 degree of freedoms by 6 independent PID controllers. The basic control structure is shown in figure 4.9.

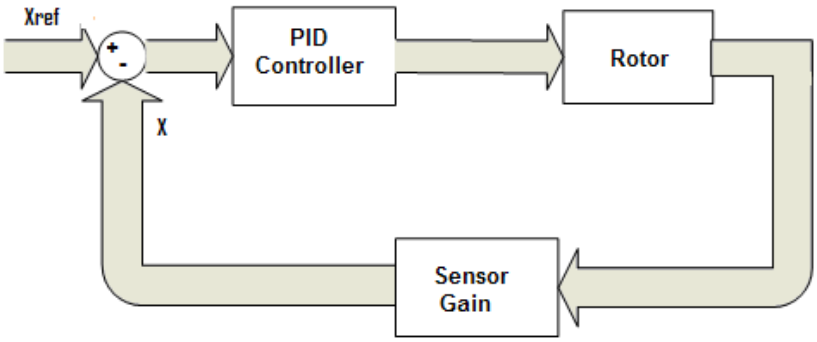

Figure 4.9 The structure of PID control system

4.2.1 PID Controller

To control the system, a proper control algorithm has to be implemented. In this system, PID controller is design as control method.

4.2.1.1 Tuning PID

As mentioned in chapter 2, a proportional-integral-derivative (PID) controller is a generic control loop feedback mechanism widely used in industrial control systems at present. A PID controller can be described as

$$u(t) = K_p e(t) + K_i \int_0^t e(\tau)d\tau + K_d \frac{d}{dt} e(t) \qquad (4.2)$$

Where K_p, K_i, and K_d are the coefficients of PID controller. The parameters of PID controller have to be well chosen in order to provide a better performance of the system. According to [14], the limitation of PID parameters is given below.

For a simple controller PD, the ideal transfer function of a PD controller is expressed as

$$G_c = K_p + sT_d \qquad (4.3)$$

The loop transfer function is

$$G_L = (K_p + sT_d) \times \frac{k_i k_{sn}}{ms^2 - k_x} \qquad (4.4)$$

The control loop of this PD controller is shown in figure 4.10. Here, k_{sn} is the sensor gain.

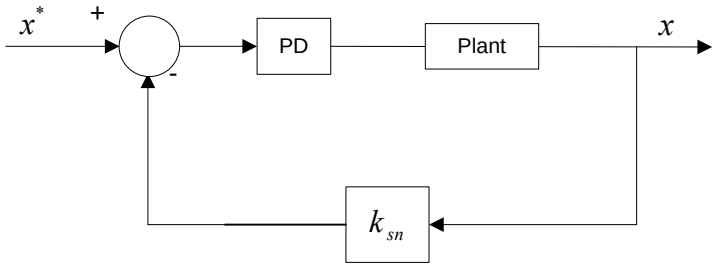

Figure 4.10 The control loop of simple PD controller

Where x is the output and x^* is the input. TF means transfer function of this system. Here, between output and input

$$\frac{x}{x*}=\frac{G_L}{1+G_L}=\frac{(K_p+sT_d)\times k_i k_{sn}}{(ms^2-k_x)+(K_p+sT_d)\times k_i k_{sn}}=\frac{(K_p+sT_d)\times k_i k_{sn}}{ms^2+sT_d k_i k_{sn}+(K_p k_i k_{sn}-k_x)} \tag{4.5}$$

From eq. (4.5), the characteristic equation is

$$ms^2+sT_d k_i k_{sn}+(K_p k_i k_{sn}-k_x)=0 \tag{4.6}$$

The roots of characteristic equation are given by quadratic formula

$$s=\frac{-k_i T_d k_{sn}\pm\sqrt{(k_i T_d k_{sn})^2-4m(K_p k_i k_{sn}-k_x)}}{2m} \tag{4.7}$$

This equation provides some conditions for the magnetic suspension stability,

a). If T_d=0 and K_P=0, then the value of numerator is equal to $\pm\sqrt{4mk_x}$. Hence, one pole is located in the right half plane. However, the system is stability when the poles of the system are located in the left plane. So the system is unstable under this condition.

b). If T_d=0 and $K_p k_i k_{sn}-k_x>0$, $num=\pm j\sqrt{4m(K_p k_i k_{sn}-k_x)}$. So two poles are located on the imaginary axis. In practice, it is not useful since it is marginally stable.

c). If T_d is positive, and $K_p k_i k_{sn}-k_x>0$,

$num=-T_d k_i k_{sn}\pm\sqrt{(k_i T_d k_{sn})^2-4m(K_p k_i k_{sn}-k_x)}$. Since two poles are located in the left plane, this system is stable.

Hence, a minimum proportional gain for the controller is $K_p > k_x / k_i k_{sn}$.

When add an external force f_d in the control loop and assume x^* is equal to zero, as shown in figure 4.11.

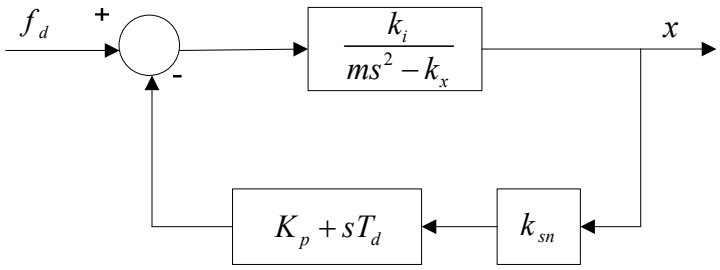

Figure 4.11 The control loop with external f_d

The transfer function of this control loop is

$$\frac{x}{f_d} = \frac{\frac{1}{ms^2 + k_x}}{1 + \frac{1}{ms^2 + k_x}[-k_i k_{sn}(K_p - sT_d]} = \frac{1}{ms^2 - T_d k_i k_{sn} s - (k_i K_p k_{sn} - k_x)} \tag{4.8}$$

The standard form of ideal second order system is

$$\frac{x}{f_d} = \frac{1}{ms^2 + k_d s + k_s} = \frac{\frac{1}{k_s}}{1 + 2\zeta \frac{s}{\omega_n} + (\frac{s}{\omega_n})^2} \tag{4.9}$$

Then, take equation (4.8) into (4.9), the expressions of ζ and ω_n are shown below

$$\zeta = \frac{T_d k_i k_{sn}}{2} \sqrt{\frac{1}{m(K_p k_i k_{sn} - k_x)}} \tag{4.10}$$

$$\omega_n = \sqrt{\frac{K_p k_i k_{sn} - k_x}{m}} \tag{4.11}$$

From equations (4.10) and (4.11), the parameters of PID controller can be tuning in some rules below:

1) Increasing derivative controller gain will get a better damping, the oscillation suppression.

2) Increasing proportional controller gain can get a fast response.

In this thesis, for radial and axial actuators the values of their PID parameters are different. According to the dimensions in chapter 3, the limitations of radial actuators and axial actuators can be calculated.

For radial actuators: $K_{p1} > 0.2$

For axial actuators: $K_{p2} > 0.2$

Moreover, from equation (4.10), derivative coefficient T_d can be presented as

$$T_d = \frac{2\zeta\sqrt{m(K_p k_i k_{sn} - k_x)}}{k_i k_{sn}} \tag{4.12}$$

Tuning PID controllers of radial and axial actuators in MATLB separately, and then, get the real value of them.

For radial actuators:
$$\begin{cases} K_{p1} = 2 \\ T_{d1} = 0.03 \\ K_{i1} = 10 \end{cases}$$

For axial actuators:
$$\begin{cases} K_{p2} = 1.9 \\ T_{d2} = 0.08 \\ K_{i2} = 10 \end{cases}$$

The closed-loop step responses of this design are shown in figure 4.12. As the figure shows, the overshoot is limited in 10% and the response time is short enough. So, the system is stable with this PID controller.

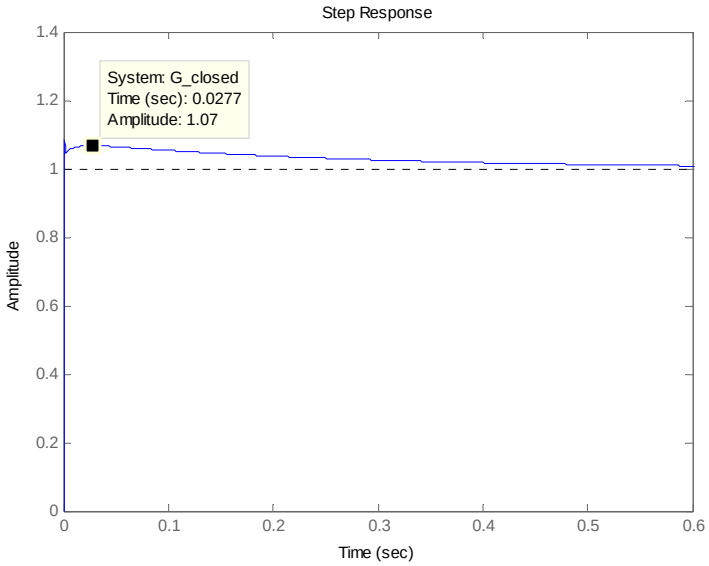

(a)

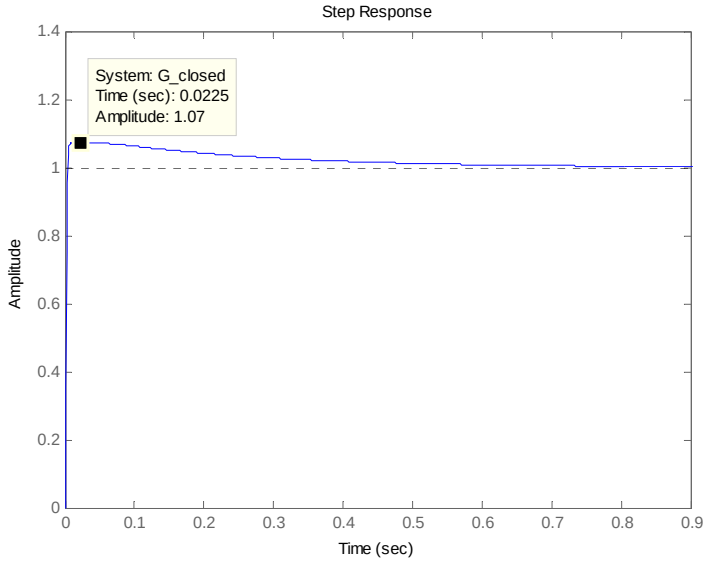

(b)

Figure 4.12 The closed-loop step response (a) is radial actuators and (b) is axial actuators

4.2.1.2 Integrator anti-windup

Although, this system is designed as a linear system as discussed before, some nonlinear effects must be accounted for in a real system. In most all systems, actuator saturates because of dynamic range of practical actuators is usually limited. Whenever control saturation happens, we have to stop integrating with the integral control law; otherwise the integrator will keep integrating, and

this charge must be removed later, resulting in substantial overshoot. This problem is called integrator windup [19]. When the integrator windup takes place, the feedback loop is broken and the system runs as an open loop.

To solve this problem of integrator windup, a number of techniques are available. In our design, back-calculation method is introduced. Back-calculation works as follows: When the output saturates, the integral term in the controller is recomputed so that its new value gives an output at the saturation limit. It is advantageous not to reset the integrator instantaneously but dynamically with a time constant T_t [20].

The system model of anti-windup controller is shown in figure 4.13. Denoting by e_i the input of integrator, it can be written as

$$e_i = eK_i + \frac{1}{T_t}(y - y') = eK_i + \frac{1}{T_t}e' \tag{4.13}$$

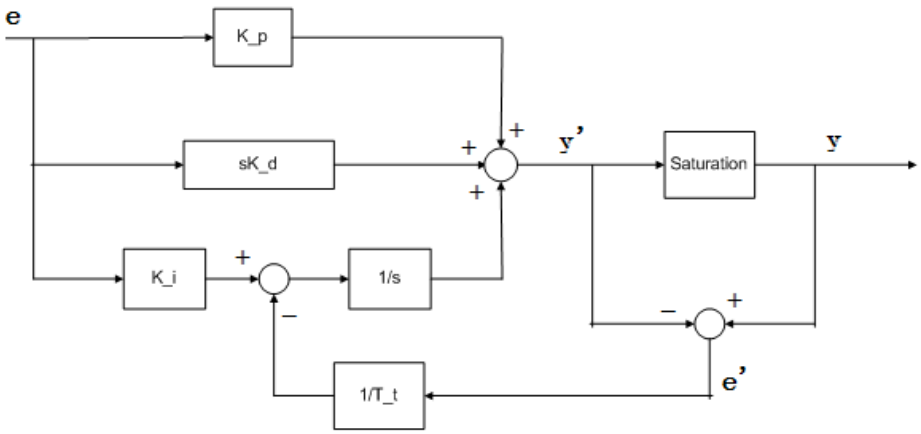

Figure 4.13 Illustration of system model with anti-windup controller

The anti-windup controller can be implemented into Simulink model, and the diagram of the controller model is shown in figure 4.14.

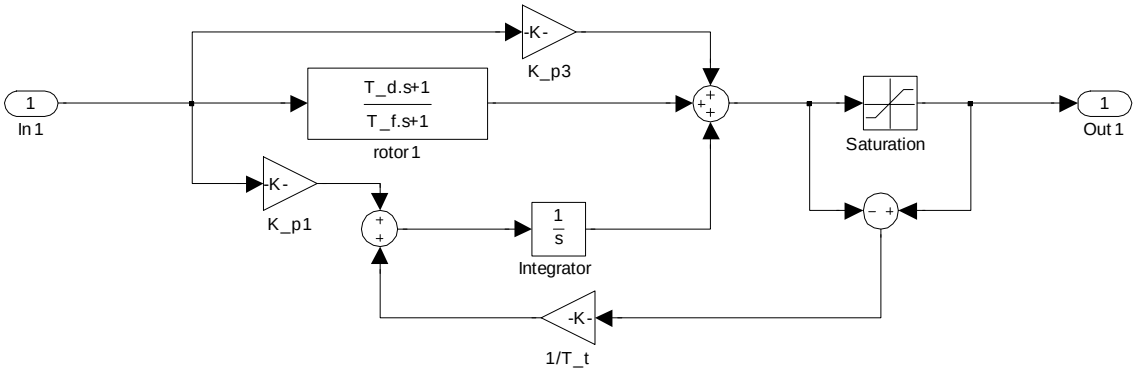

Figure 4.14 Diagram of anti-windup controller in Simulink

This integral anti-windup controller is not implemented in this thesis. Because this system is designed as a linear model, but the saturation block is nonlinear. So when we add this integral anti-windup controller in the system, it is no longer steady. For a first levitation of the magnetic bearing setup, considering a linear model is enough. When improvement this control system to control the rotor in five degree of freedoms, the integral anti-windup maybe useful.

4.2.2 Decentralized Control

This thesis discusses a closed loop decentralized control for active magnetic bearings. Decentralized control means the rotor is controlled by 6 independent PID controllers. So decentralized control is also called “local” control. As shown in figure 4.15(a), the term "local" implies the following concepts: sensor "1" and bearing "1" form the subsystem "1", and the others are formed in the same way. The sensors are each assigned to a bearing unit. Figure 4.15(b) shows a different control structure which is called central control. Central control is more complex and difficult to implement than decentralized control. The rotor will be controlled in five degree of freedoms by only one controller.

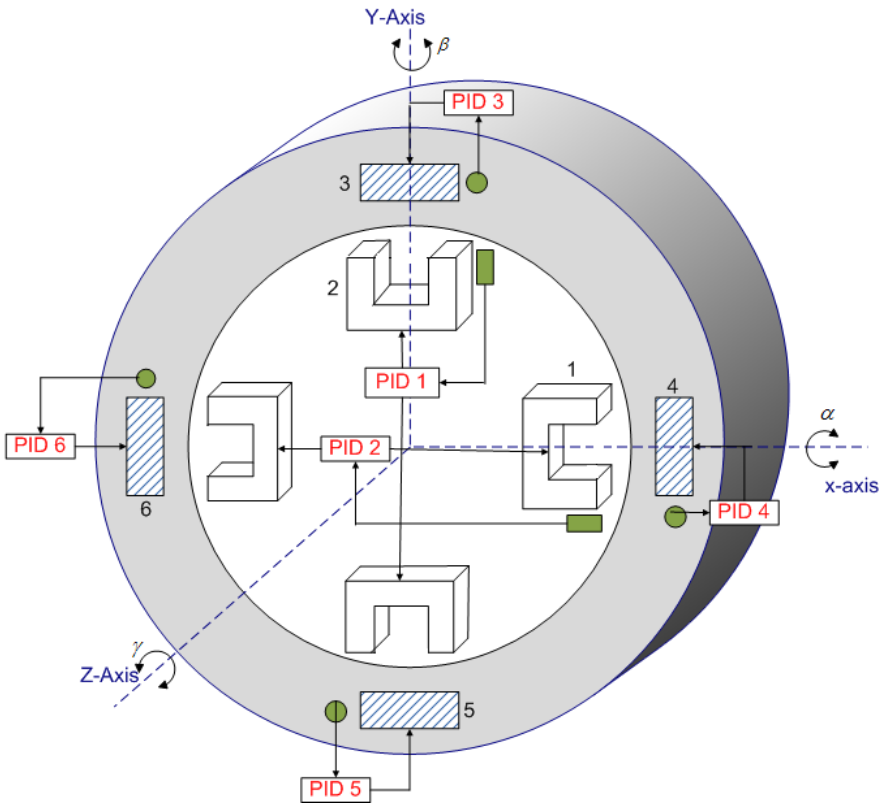

(a)

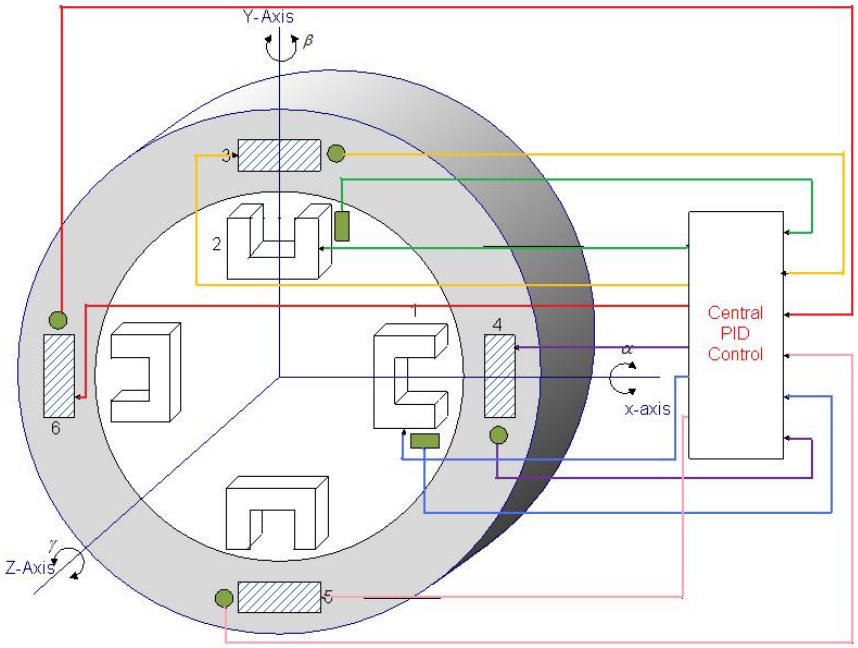

(b)

Figure 4.15 The structure of control system with PID controller

(a) is decentralized control and (b) is central control

The biggest advantage of decentralized control is the control parameters that can be designed solely based on physical considerations by selecting appropriate stiffness and damping values. Moreover, in decentralized control the closed loop AMB system will feature acceptable performance and robustness properties [10].

This decentralized control design can be implemented in simulation as shown below: There are six PID controller subsystems for each sensor and bearing. Six signals are controlled by local PID controllers, and then, combined into the matrix of rotor model.

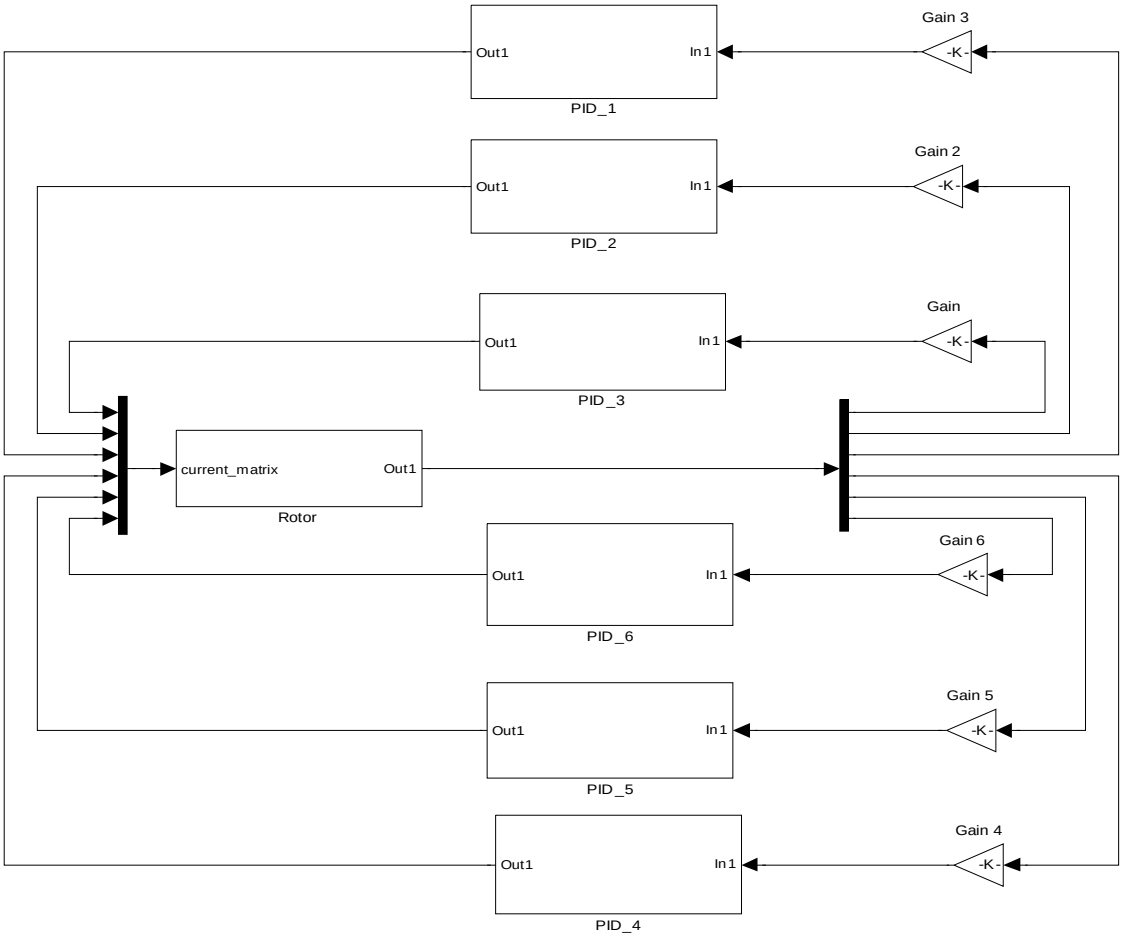

Figure 4.16 Simulink of decentralized control

As discussed in chapter 3, equation (3.23) can be expressed in

$$M_1 \frac{d^2 X_{1...6}}{dt} = M_2 X_{1...6} + M_3 I_{1...6} \tag{4.14}$$

Where, M_1 is mass matrix, M_2 is force/displacement matrix and M_3 is force/current matrix. $X_{1...6}$ and $I_{1...6}$ are position and current matrix of six signals.

Equation (4.14) can be written as

$$\frac{d^2 X_{1...6}}{dt^2} = M_1^{-1} M_2 X_{1...6} + M_1^{-1} M_3 I_{1...6} \tag{4.15}$$

Let $Y_{1...6} = \frac{dX_{1...6}}{dt}$, then the equation (4.16) can be expressed below

$$\begin{cases} \dfrac{dY_{1...6}}{dt} = M_1^{-1} M_2 X_{1...6} + M_1^{-1} M_3 I_{1...6} \\ Y_{1...6} = \dfrac{dX_{1...6}}{dt} \end{cases} \tag{4.16}$$

Equation (4.16) can be written in state-space, as shown below

$$\begin{bmatrix} \dot{Y}_{1...6} \\ Y_{1...6} \end{bmatrix} = \begin{bmatrix} 0 & M_1^{-1} M_2 \\ 1 & 0 \end{bmatrix} \begin{bmatrix} \dot{X}_{1...6} \\ X_{1...6} \end{bmatrix} + \begin{bmatrix} 0 & M_1^{-1} M_3 \\ 0 & 0 \end{bmatrix} \begin{bmatrix} \dot{I}_{1...6} \\ I_{1...6} \end{bmatrix} \tag{4.17}$$

Implemented equation (4.17) into Simulink, the rotor model with matrix can be represented below, which is also shown in figure 4.17 as rotor subsystem.

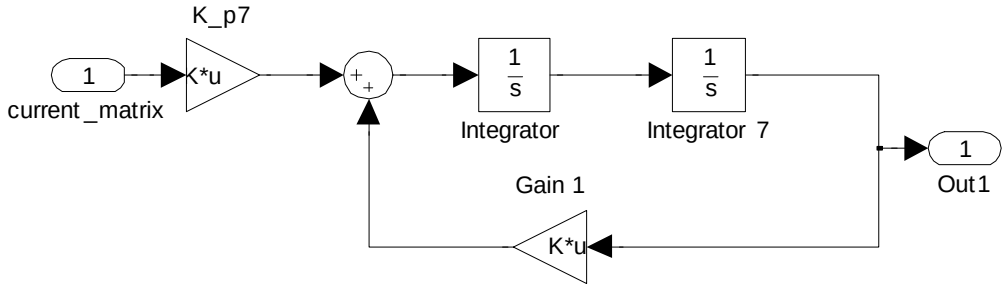

Figure 4.17 Rotor model in Simulink

Chapter 5 Measurements and Results

In the previous chapters, a complete control system for magnetic bearings was designed. And then, this chapter talks about the performance of the setup and some measurement results. In section 5.1, the setup of this magnetic bearing system is introduced, including hardware and PCB design. Then in section 5.2, some analyses of performance using the setup are shown.

5.1 Setup of Magnetic Bearing System

In our design, a completed setup of magnetic bearing system is comprised of actuators, sensors, rotor, amplifiers, two PCBs, and a DSP. The schematic of this magnetic bearing system is shown in figure 4.1. Based on that block, the real setup is built. The real pictures of this setup are shown in following.

5.1.1 Sensors

In our design, micro epsilon eddy current sensor is used. The type of the sensor is eddy NCDT 3010 (non-contact eddy-current displacement and position measurement). To control the rotor in 5 degree of freedoms, six such sensors are used in this magnetic bearing system.

The sensor measures the displacement of the rotor from its reference position, and produces a linear electrical signal proportional to the distance of the rotor from the sensor. In our design, the electrical signal output is 5V/mm. The power supply for this sensor is 24VDC/205mA. Figure 5.1 gives a picture of such kind of sensor.

Figure 5.1 Eddy current sensor

5.1.2 Two PC Boards

As discussed in section 4.1, there are two boards are designed in this measurement system.

The first board, which from sensor output to DSP input, is shown in figure 5.2. The power supply to this board is 24VAC.

Purple block is the signal circuit with 12 resistors. Two resistors compose to one group for transferring one signal from 10V to 3V, which is DSP required.

The blue cycles indicate the diode bridge, which is used to rectifier the AC voltage to DC voltage.

Filter part is shown in red block, with 2 op-amps and six groups of resistors and capacitors. It is used to keep the signal in a certain frequency range.

The voltage regulators are indicated in green block. They are used to support the power supply to sensors and op-amps.

The pink cycle transfers 24DC voltage to 15DC voltage, which is used to support the other board in this system.

The second board is shown in figure 5.3, which from DSP output to amplifier. The power supply for this board is got from the first board.

In this board, there are six opto couplers to get 12 isolated PWM signals. The power supply for opto coupler is 15VDC, which transferred by dc-dc converter as shown in orange cycle in the picture.

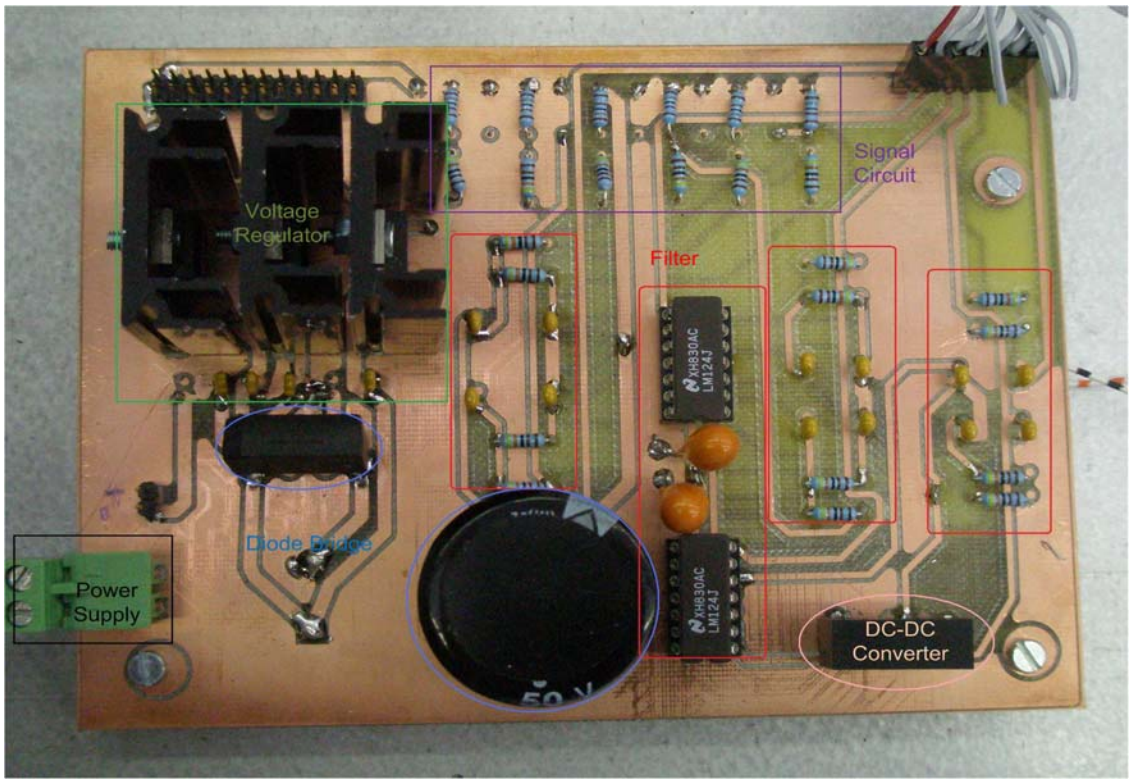

Figure 5.2 PCB_1 from sensor output to DSP input

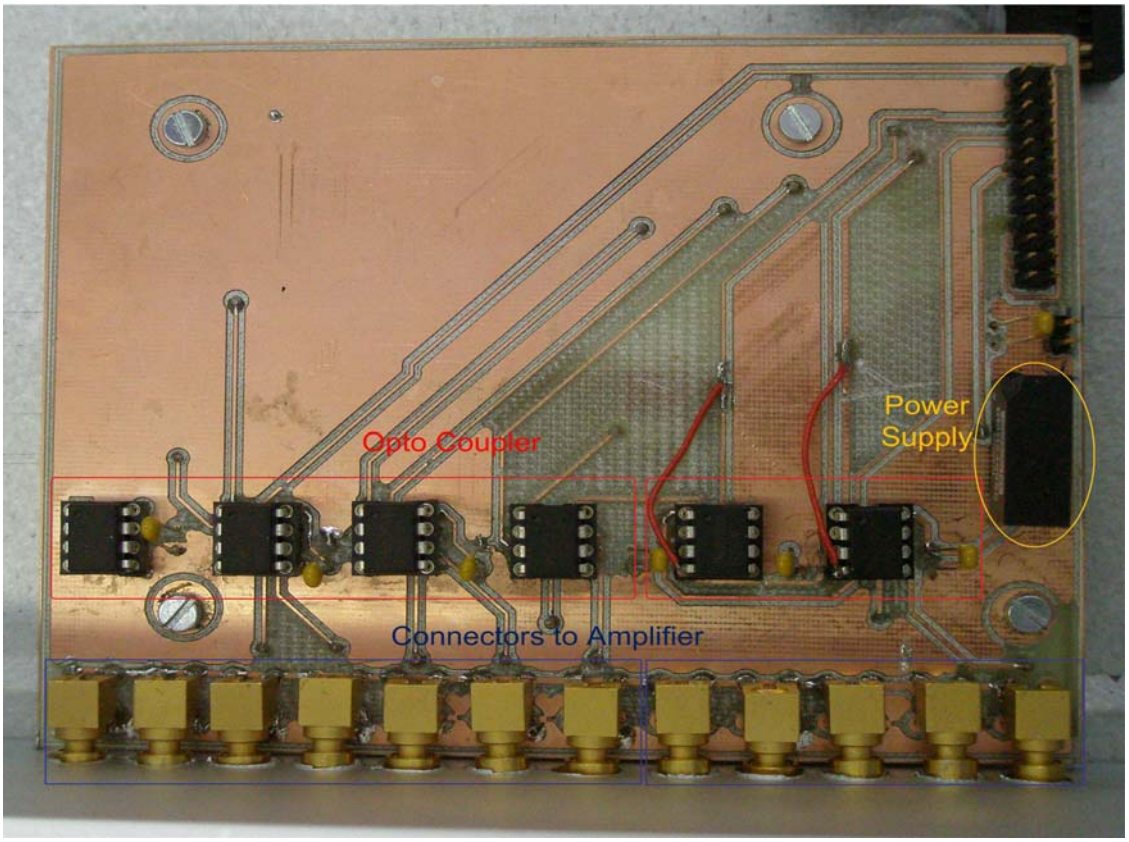

Figure 5.3 PCB_2 from DSP output to amplifier

5.1.3 DSP

In our design, the designed control method is implemented into one Digital Signal Processor (DSP) to control the magnetic bearing system. The type of this DSP is eZdsp^{TM} F2808 USB. This DSP is powered by a 3.3 volt external power supply, and requires a 500mA current.

5.1.4 Amplifiers

Depending on the differential mode of actuator design, we have 12 current signals input to the actuator. Each current needs one amplifier. So, 12 AZ12A8 PWM amplifiers are used in this project, as shown in figure 5.4. The AZ121A8 is fully protected against over-voltage, over-current, over-heating, and short circuit. To increase system reliability and to reduce cabling costs, the drive is designed for direct integration into PCB. The supply voltage of this kind of amplifier is 20-80VDC, continues current is 6A, and the peak current is 12A.

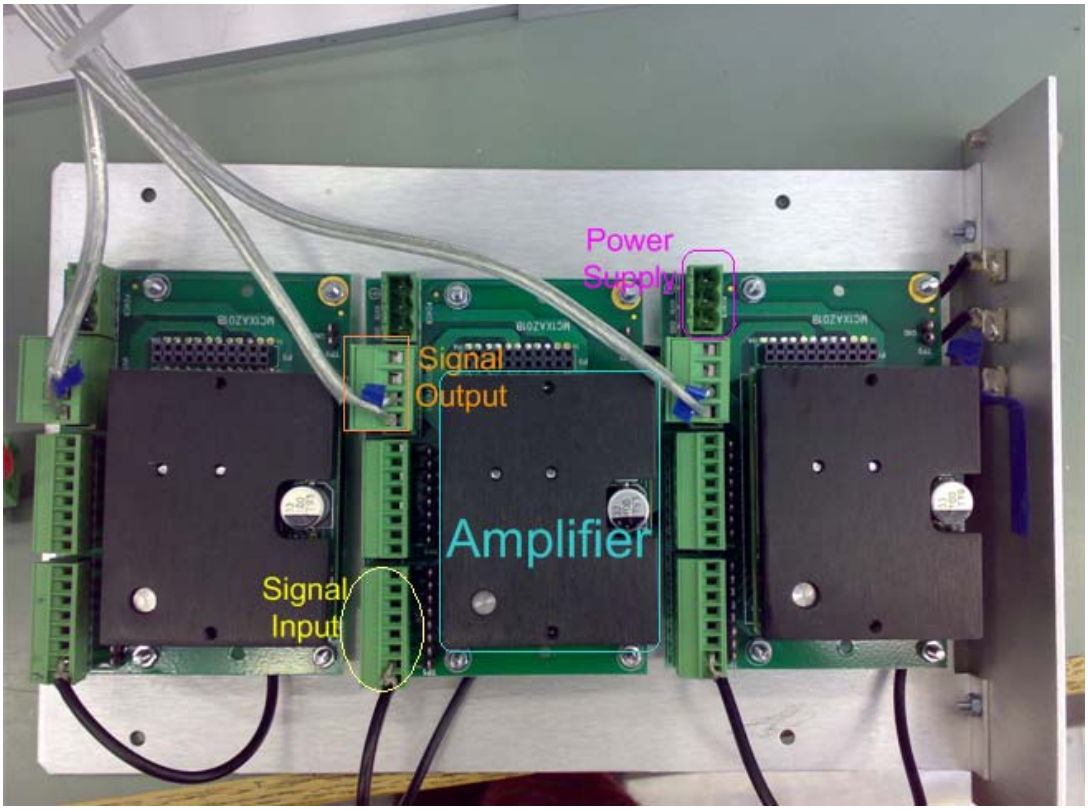

Figure 5.4 AZ12A8 PWM amplifiers

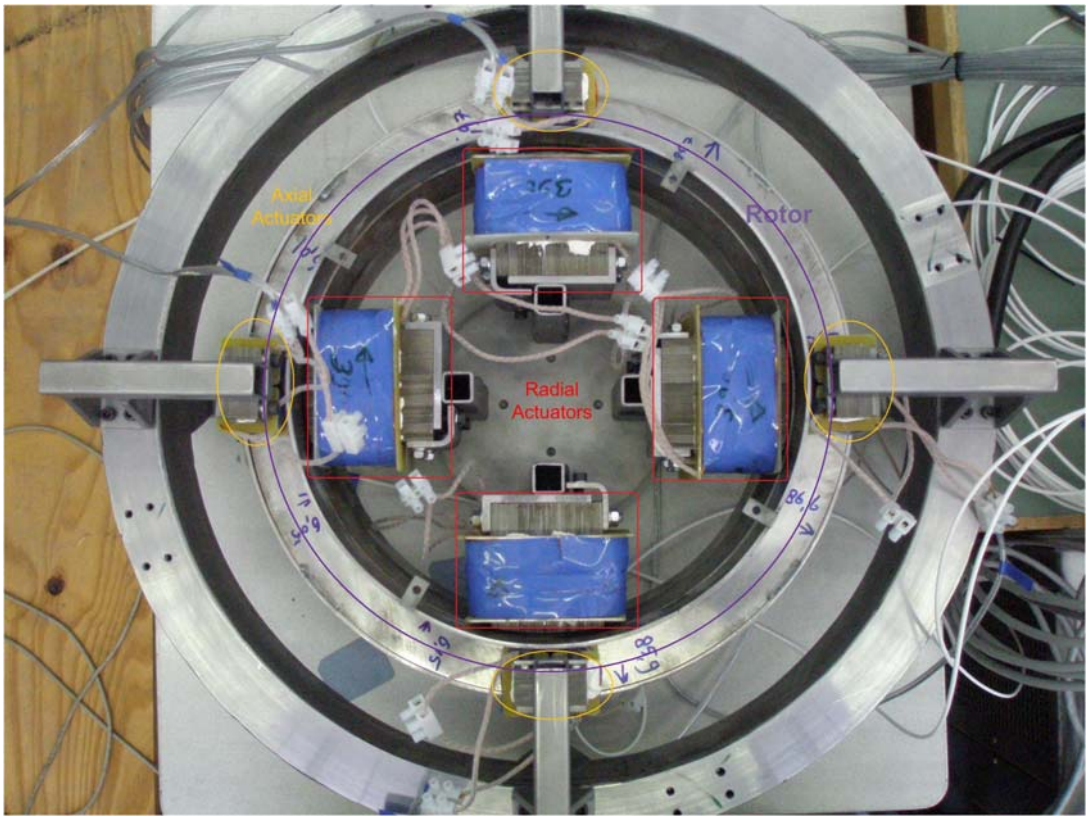

Figure 5.5 The rotor and actuators of this system.

5.1.5 Rotor and Actuators

In our design, the rotor is controlled by six pairs of actuator. Amongst them, two pairs are radial actuators as shown in figure 5.5 within red blocks. The orange cycles indicate four pairs of axial actuators. In the picture, we can see four axial actuators on the top of rotor, and the other four axial actuators are under the rotor.

The signals from amplifiers output induce the current in these actuators are used to take the rotor back to the right position.

5.2 Results

5.2.1 Simulation Results

As discussed before, this thesis starts from one degree of freedom. The simulation model of one degree of freedom is shown in figure 5.6. The results of radial actuators and axial actuators are shown in figure 5.7 and 5.8. In one degree of freedom control, we try to tuning the PID coefficients, within a limitation as we discussed in chapter 4, to make the system stable. The amplifiers in this thesis can be provided by 6A, and the peak current is 12A. As shown in figure 5.7 and 5.8, the current need to be transferred to analog value by multiple a factor12/6400. The currents input to amplifiers are all limited in 12A.

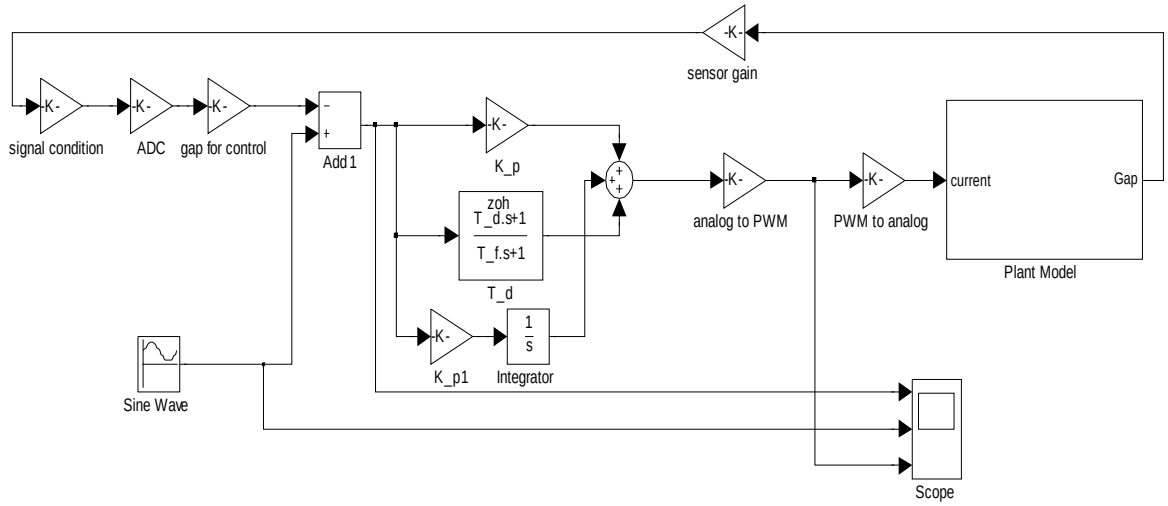

Figure 5.6 Simulation model of one degree of freedom

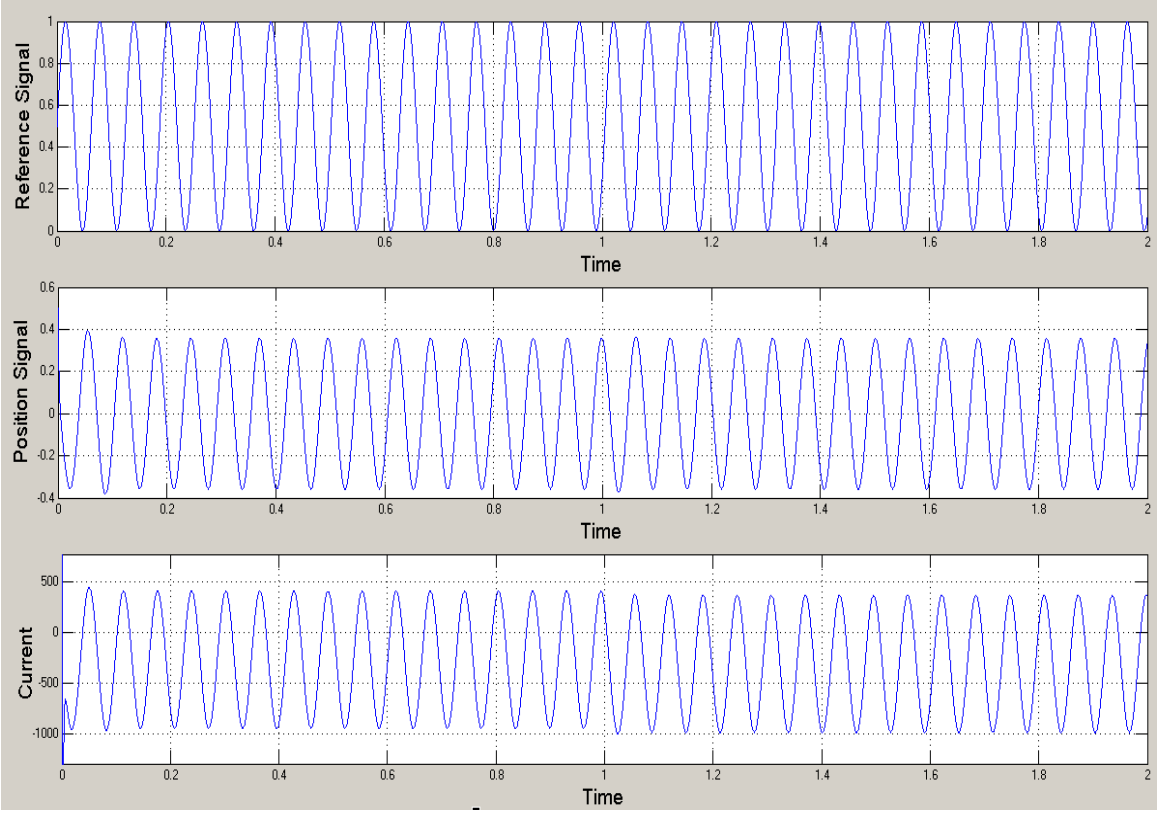

Figure 5.7 One degree of freedom control of radial actuators

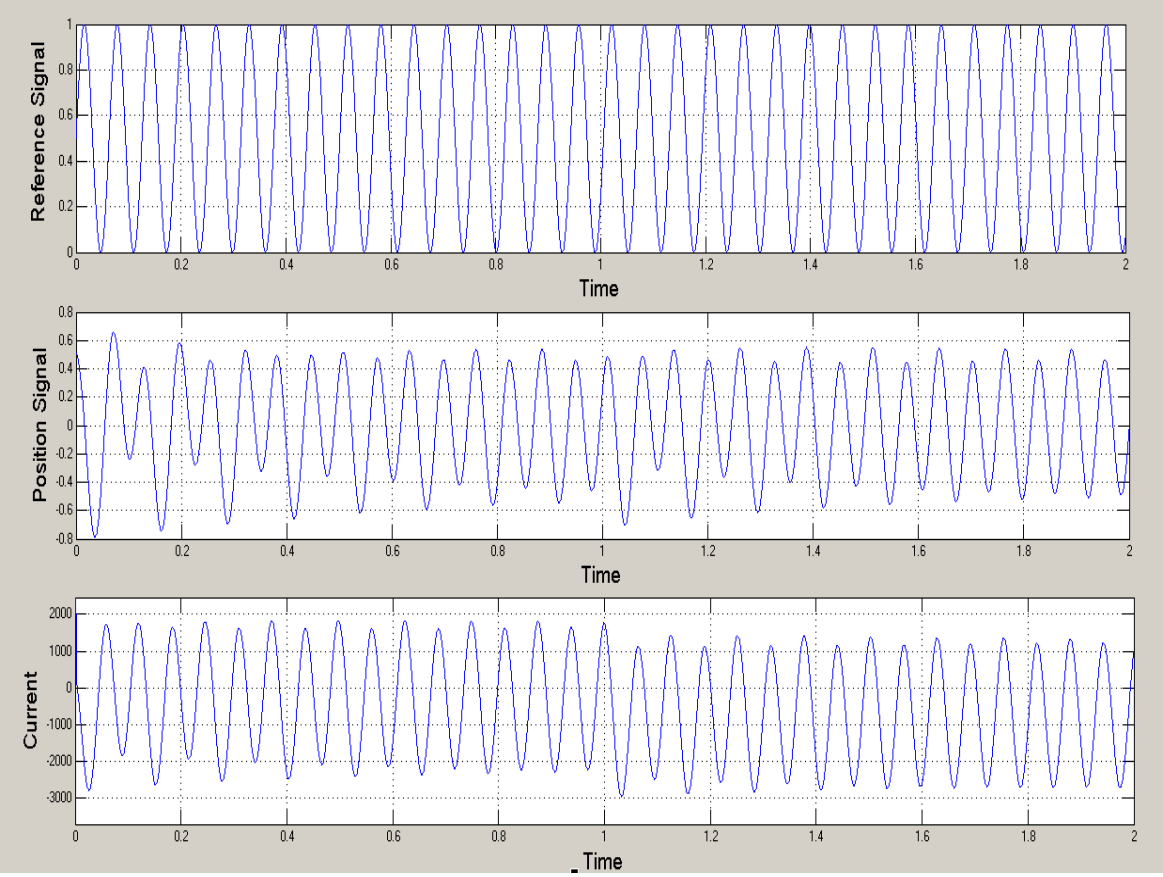

Figure 5.8 One degree of freedom control of axial actuators

For the purpose of get the first levitation of the demonstrator, we use four pairs of axial actuators to eliminating the gravity of the rotor. As discussed in chapter 3, the actuators are designed in differential model, which means give a bias current into the model. This differential model is shown in figure 5.9. In order to eliminate the gravity of the rotor, the force in upper actuators are bigger than the below ones. Therefore, the bias current in upper side is i_0+i_g.

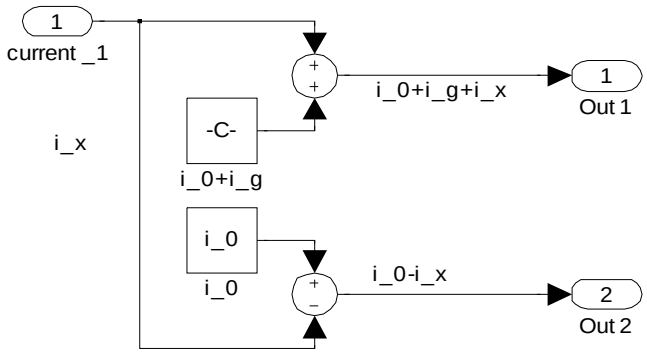

Figure 5.9 Differential models in simulation

In our design, we start to levitate the rotor from simple PD controller as shown in figure 5.10, and the levitation model is shown in figure 5.11. The PD controllers control each pairs of axial actuators separately.

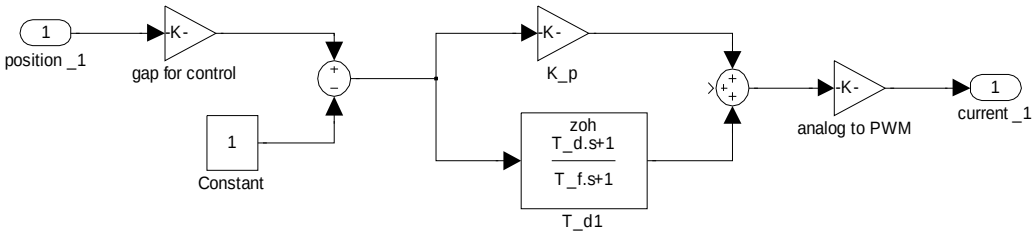

Figure 5.10 PD controllers in simulation

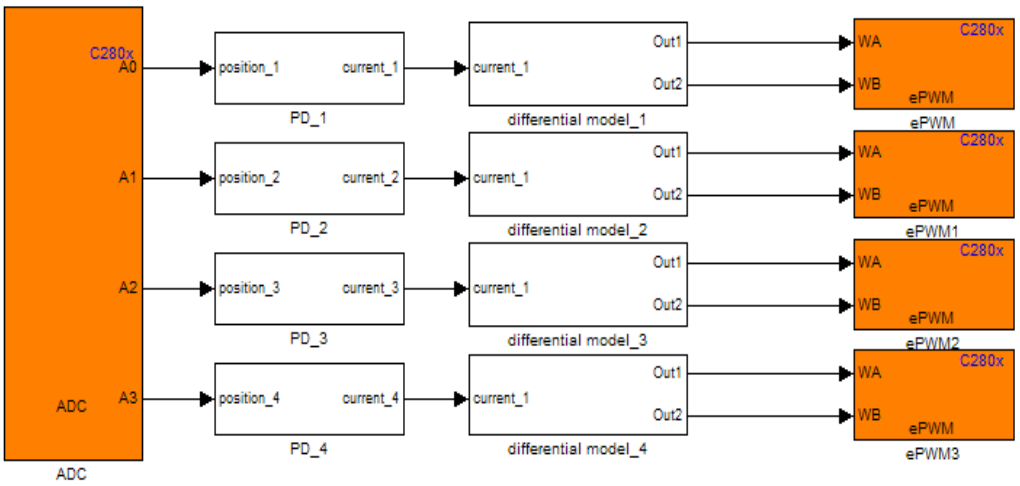

Figure 5.11 Levitation model in simulation

Chapter 6 Conclusion

This thesis starts from two types of generators used in wind turbines. Compared these two kinds of generators, active magnetic bearing is introduced to improve the direct drive generator.

As mentioned in section 1.3, active magnetic bearing has a lot of advantages which maybe reduce the weight of direct drive wind turbines. Based on this concept, we need a control system to support magnetic bearings in wind turbines.

This thesis project is focused on the control system design of magnetic bearings in wind turbines. We pay more attentions on different types of magnetic bearings and choose decentralized control with PID controllers in this thesis. In our system, the rotation speed of the rotor is not too high, so we don't consider gyroscopic effect in the rotor model.

According to decentralized control method, the rotor model is built based on six positions from six sensors separately. As experience, the magnetic bearings are mostly used in differential model, which is possible to generate both positive and negative forces. And then the actuator is designed linearized.

After modeling the actuator and the rotor, a completed control system is needed to control the rotor in five degree of freedoms. This completed control system includes both electronic circuit part and control part. The electronic circuit part is designed into two PCBs, and the control part is designed in decentralized control with six PD controllers.

Based on the design of the system, implemented the control system design into the Simulink and the real setup.

For the first levitation of the rotor, we use four PD controllers to control the axial actuators. We tuning the coefficients of the PD controllers individually, and it is levitation. However, without the integrated part, there is a state error in the system. If we need control the rotor in five degree of freedoms, the integrate part needs to be considered.

The contribution of this thesis is practical design of control system for magnetically levitated generator.

Reference

[1] http://en.wikipedia.org/wiki/Offshore_wind

[2] G. Shrestha, H. Polinder, D.J. Bang, J.A. Ferreira; "Structural Flexibility: A Solution for Weight Reduction of Large Direct Drive Wind Turbine Generators"

[3] G. Shrestha, H. Polinder, D. Bang, A.K. Jassal, J.A. Ferreira; “Investigation on the Possible Use of Magnetic Bearings in Large Direct Drive Wind Turbines”

[4] Versteegh C.J.A.; “Design of the Zephyros Z72 wind turbine with emphasis on the direct drive PM generator”, NORPIE 2004.

[5] Eric H. Maslen, Gerhard Shcweitzer; “Magnetic Bearings Theory, Design, and Application to Rotating Machinery”

[6] Engstrom A. S., Lindgren S.; “Design of NewGen direct drive generator for demonstration in a 3.5 MW Wind Turbine”, EWEC 2006

[7] Stanley M.Shinners; "Modern Control System Theory and Design"

[8] E. Gottzein, L. Miller, and R. Meisinger; “Magnetic suspension control system for high speed ground transportation vehicles”, In World Electrotechn. Congr., Moscow, June 1977

[9] http://en.wikipedia.org/wiki/Maglev_(transport)

[10] Schweitzer, G. Bleuler, H. Traxler; “Active magnetic bearings”; 1994

[11] Suyuan Yu, Guojun Yang, Lei Shi, and Yang Xu; “Application and research of the active magnetic bearing in the nuclear power plant of high temperature reactor”; In H. Bleuler and G. Genta, editors; Proc. 10th Internat. Symp. In Magnetic Bearings, page keynot, Martigny, Switzerland, Aug. 2006

[12] Chen, C. Paden, B. Paden, D. Antake, J. Ludlow, J. Bearnson, G. Crwonson, R.2001; “A magnetic bearing suspension theory and its application to the HeartQuest Ventricular assist device”; 9th Congress of the International Society for Rotary Pumps, Seattle, Washington, Aug.2001

[13] Araki. M; "PID control"; Kyoto University, Japan

[14] Akira Chiba, Tadashi Fukao, Osamu Ichikawa, Masahide Oshima, Masatugu Takemoto; "Magnetic Bearings and Bearingless Drive"

[15] http://en.wikipedia.org/wiki/Opamp

[16] Thomas Kugelstadt, “Active Filter Design Techniques”

[17] Gerhard Schweitzer; “Applications and Research Topics for Active Magnetic Bearings”; Switzerland

[18] Kerry lacanette, “A Basic Introdution to Filters – Active, Passive, and Switched - Capacitor”, National Semiconductor Application Note 779, April 1991

[19] Gene F. Franklin, J. David Powell, ABBAS Emami-Naeini; “Feedback Control of Dynamic Systems”; third edition
[20]Karl Johan Astron; “Control System Design”; Chapter 6 PID control; 2002
[21] H. Houpis, Steven J. Rasmussen; “Quantitative feedback theory: fundamentals and applications”; 1999
[22] Dapeng Wang, Fengxiang Wang and Haoran Bai; “Design and Performance of QFT-H-infinity Controller for Magnetic Bearing of High-Speed Motors”; IEEE 2009
[23] http://en.wikipedia.org/wiki/Step_response
[24] H. Polinder, F.F.A. van der Pijl, G.J. de Vilder, P. Tavner; “Comparison of direct-drive and geared generator concepts for wind turbines”; IEEE Trans. Energy Conversion, Vol. 21, pp. 725-733, September 2006
[25] D. Bang, H. Polinder, G. Shrestha, J.A. Ferreira; “Review of Generator Systems for Direct-Drive Wind Turbines; Electrical Power Processing / DUWIND, Delft University of Technology

Appendix

The schematic of the board into DSP

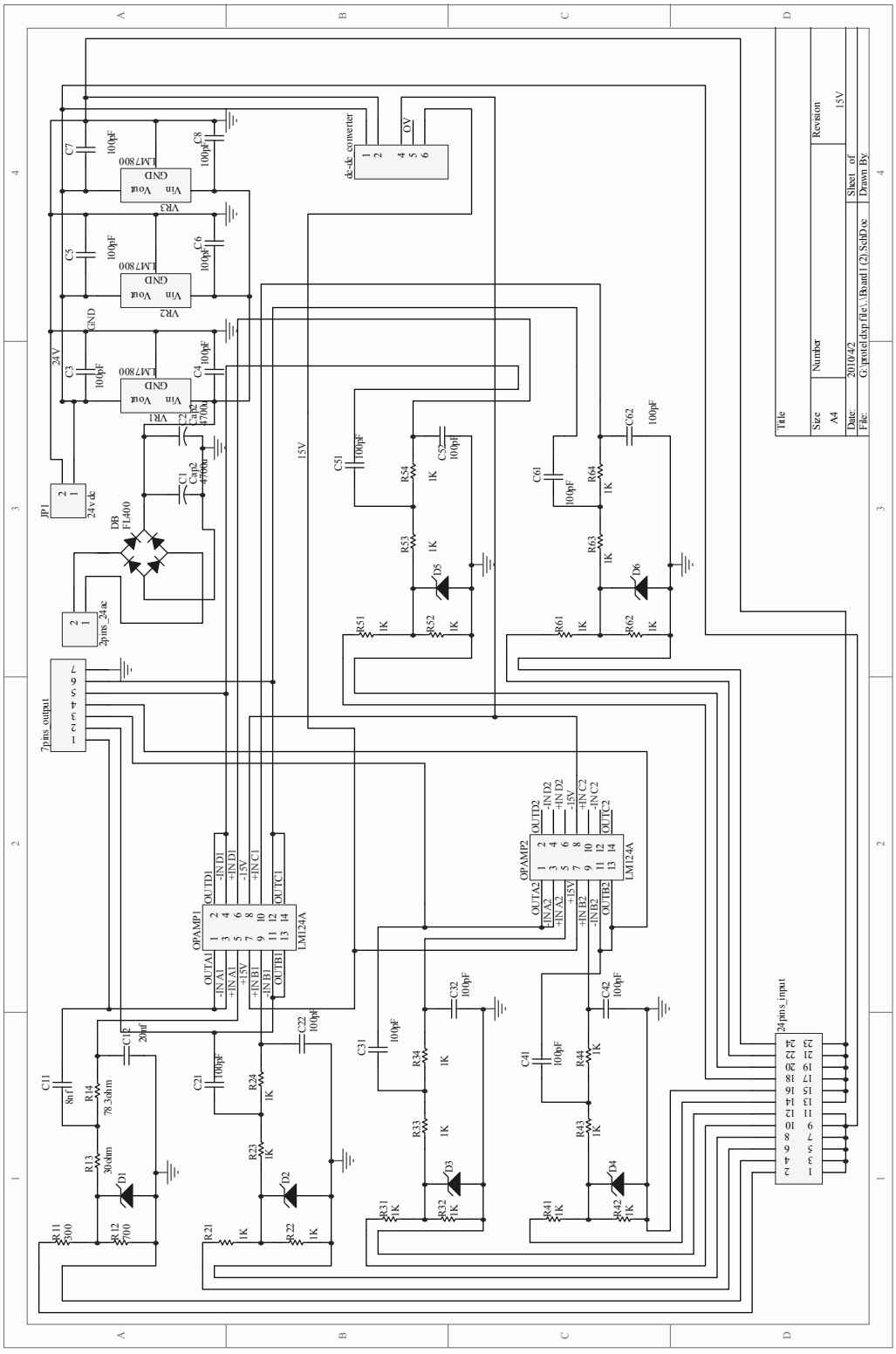

The schematic of the board into amplifiers

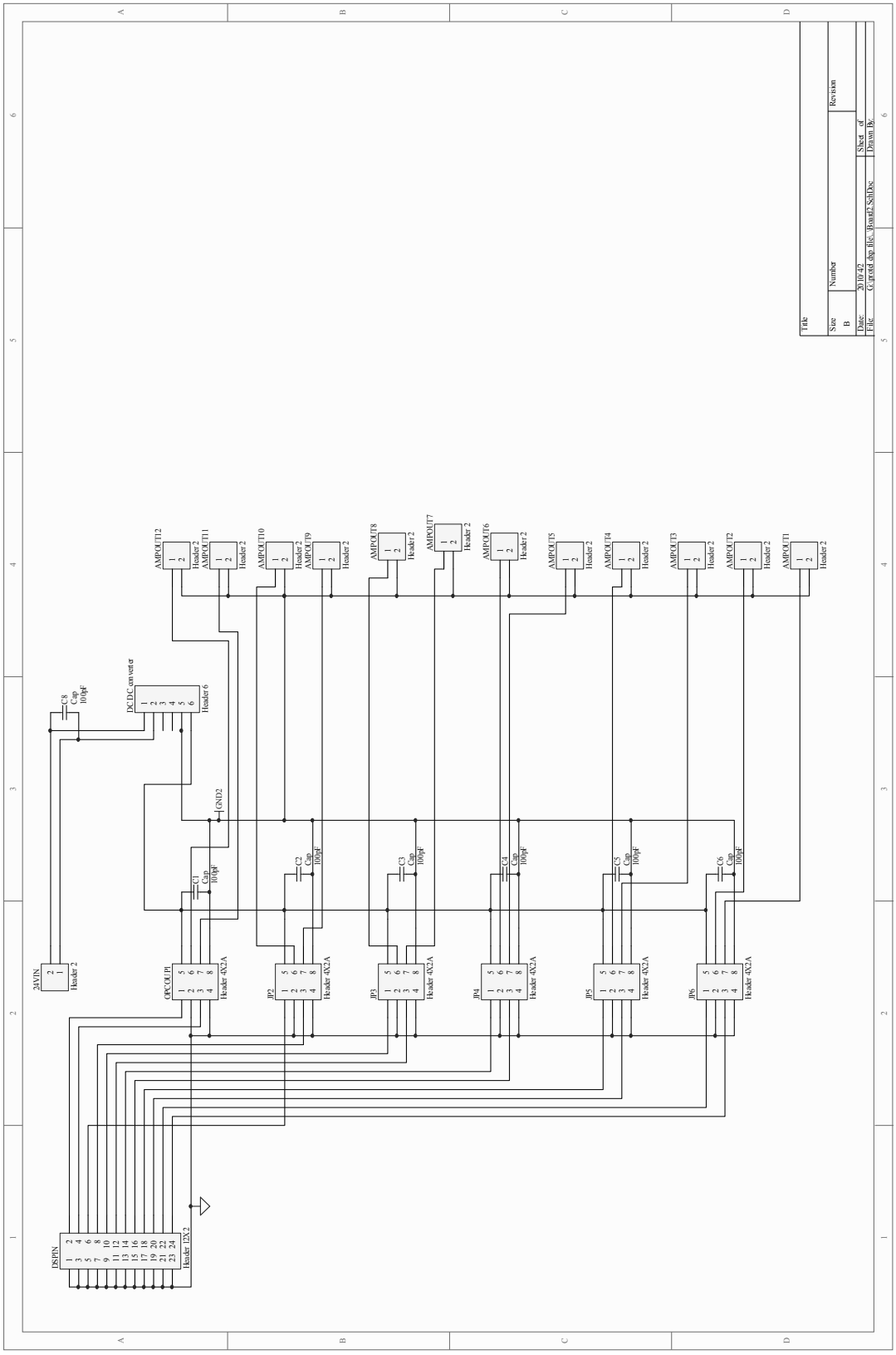

PCB layout of the board into amplifiers